A Robust Load Adaptability Method to Suppress AC Harmonic for Series-Connected 12-Pulse Rectifier With DC Side Active Harmonic Injection Circuit

Ruidong Sun, *Student Member, IEEE*, Guohong Zeng, Buyu Yang, Luoqi Wu, Wenzheng Xu, Long Jing, Xuezhi Wu, *Member, IEEE*, Jianhua Lei, and Yongbo Zhang

***Abstract*—Though the dc side harmonic reduction methods of multipulse rectifiers can improve ac side power quality, they are applicable only to large inductive load. This article proposes a novel active harmonic injection circuit (AHIC) for a series-connected 12-pulse rectifier to achieve lower input current total harmonic distortion (THD) with a nonideal inductive load. First, the harmonic suppression effect of two representative passive and active harmonic reduction circuits under load ripple current conditions is analyzed, and the mechanism of poor load adaptability is revealed. On this basis, the AHIC realized by two-stage dc-ac-ac three-port converter is installed at dc side as two independent current sources. By extracting harmonics from load current and superimposing them on original triangular current, the AHIC generates specific injection circulating currents to offset the undesired harmonics of rectifier output current. The resulting rectifier draws a near-sinusoidal input current with less than 3% THD during complex conditions. The proposed AHIC has the merits of low voltage stress ($5\%U_{\mathrm{dc}}$), small design capacity ($2.5\%P_{\mathrm{L}}$), and elimination of the necessary magnetic devices of existing methods. An experimental prototype is established to validate the performance of proposed rectifier.**

***Index Terms*—12-pulse rectifier, active harmonic injection circuit (AHIC), dc side harmonic reduction method, input current total harmonic distortion (THD), load adaptability.**

I. Introduction

THE series-connected 12-pulse rectifier, which has significant advantages in structure, reliability, overload capacity, and efficiency, is a preferred interface converter between medium/high-voltage dc power systems and grid, such as aerospace, marine, and rail transit [1], [2], [3]. However, its ac current total harmonic distortion (THD) exceeds 10%, which does not meet the relevant IEEE standards [4]. Various methods for reducing the input current THD can be classified into three types according to the location of improved measure taken. The first type employs ac side active power filters (APFs) to compensate input current harmonics [5], [6], [7]. However, the APFs have large capacity, high cost, and complex control [8]. The second method increases the pulse number by subdividing the phase-shifting transformer's output voltage phases [9], [10], [11], [12]. Increasing the pulse number can suppress current harmonics, but the rectifier construction becomes complex and difficult to fabricate, raising the volume and cost [13]. In the third group, the harmonic reduction circuits (HRCs) are installed at dc side to obtain better performances by reshaping output voltage or current of the rectifier [14]. These methods have attracted the attention of scholars with the advantages of simple circuit, small capacity, easy implementation, and better application prospects.

Available dc side harmonic reduction methods are mainly classified to harmonic injection method and output current modulation method. To improve the current quality without increasing complexity, a 24-pulse rectifier with a square-wave current injection passive auxiliary circuit (SCIPAC) was proposed in [15] and [16]. The specific square-wave currents are injected equally into the outputs of two three-phase bridge rectifiers (TPBRs) through an interphase reactor (IPR), and then the input current steps are doubled to 24. However, the auxiliary diodes in series with the load have large current stress and loss. To address this issue, Wang et al. [17], [18], [19] proposed a series of quasi 24-pulse rectifiers employing the SCIPACs in parallel with load. Increasing the rectifier working modes multiplies the ac current steps to 24. Specifically, Wang et al. [19] used the passive current injection circuit based on dual auxiliary transformers (PCIC-DAT) to reduce the magnetic device capacity. Unfortunately, these methods have limited harmonic suppression with the optimized input current THD is even 7.57%. In [20], a 36-pulse rectifier combines a series-type SCIPAC in [15] with a parallel-type SCIPAC in [17]. Meanwhile, Choi et al. [21] and Villablanca et al. [22] have replaced diodes with thyristors, increasing auxiliary transformer taps and thyristors to boost ac current steps from 12 to 36, 48, and more, but this raises system size, cost, and control complexity. In order to further reduce the input current THD, Meng et al. [23], [24], [25], Du et al. [26], and Li et al. [27] proposed a series of current source multipulse

Received 10 December 2024; revised 1 April 2025; accepted 25 April 2025. Date of publication 1 May 2025; date of current version 30 June 2025. This work was supported by the Shenzhen Science and Technology Plan Project under Grant KJZD20230923112959001. Recommended for publication by Associate Editor P. Karamanakos. *(Corresponding author: Long Jing.)*

Ruidong Sun, Guohong Zeng, Buyu Yang, Luoqi Wu, Wenzheng Xu, Long Jing, and Xuezhi Wu are with National Active Distribution Network Technology Research Center, Beijing Jiaotong University, Beijing 100044, China (e-mail: 20117025@bjtu.edu.cn; ghzeng@bjtu.edu.cn; 24121353@bjtu.edu.cn; 22121528@bjtu.edu.cn; xuwenzheng@bjtu.edu.cn; ljing@bjtu.edu.cn; xzhwu@bjtu.edu.cn).

Jianhua Lei and Yongbo Zhang are with Shenzhen Poweroak Newener Company Ltd, Shenzhen 516083, China (e-mail: leijh@poweroak.net; zhangyb@poweroak.net).

Color versions of one or more figures in this article are available at https://doi.org/10.1109/TPEL.2025.3566208.

Digital Object Identifier 10.1109/TPEL.2025.3566208

rectifiers based on dc side voltage injection circuits by adding large filter inductors to ac input. Compared to the 24-pulse rectifier in [19], the current source 24-pulse rectifier in [23] reduces input current THD from 5% to 2.65%. But, large input inductors decrease the rectifier displacement factor and make the output voltage characteristic very soft, which is unsuitable for applications with high supply voltage quality.

Modulating two TPBRs output currents with the DC side active auxiliary circuits is another effective method to suppress input current harmonics. In [28], a low harmonics 12-pulse rectifier is reported, using active switching devices in series with the dc output to shape TPBRs currents into triangle. A 12-pulse rectifier using active switches isolation is proposed in [29], keeping the TPBR output current in boundary of continuous and discontinuous conduction. Then, the input current is corrected to near-sinusoidal, but active switches endure high current stress and serious conduction loss. Further, a 12-pulse rectifier employing a cascaded buck-boost converter in parallel with the load modulates TPBRs output currents to suppress harmonics [30]. This method exploits the dc filters design to minimize auxiliary circuit volt-amperes (VA) rating, but it suffers from high voltage stress, complex control, and large dc filters. In [31], a 12-pulse rectifier with auxiliary voltage source circuit is developed to reduce the active component stress, but its ac input also requires inductors. Referring to a parallel-connected 12-pulse rectifier with an auxiliary current source circuit (ACSC) in [32] and [33], a series-connected 12-pulse rectifier uses ACSC to modulate the input current into near-sinusoidal waves via controlled circulating currents [14]. However, the heavy magnetic devices bring obstacles to the miniaturized design of the rectifier [19].

Through a comprehensive analysis of dc side harmonic reduction methods, active current modulation demonstrates better harmonic suppression compared to passive harmonic injection, providing greater flexibility and eliminating the dependence on passive device parameters. It is worth noting that most methods are discussed under a large inductive load with a constant dc current. However, dc power systems exhibit complex load characteristics, and the effectiveness of existing dc side HRCs when there are ripple currents in the load remains unverified. In [34], the load adaptability of a parallel-connected 12-pulse rectifier with active IPR has been studied, finding that the input current THD is affected under *RC*-type load, and its load adaptability can be improved by adding an *LC* filter.

To explore the load adaptability of the dc side harmonic reduction methods for a series-connected 12-pulse rectifier, two types of load conditions are considered, which can induce ripple current. Meanwhile, the harmonic suppression under nonideal load conditions is analyzed with two representative dc side HRCs as examples, to reveal the essence of the impact on load adaptability. To overcome the drawbacks of the existing schemes, a series-connected 12-pulse rectifier with active harmonic injection circuit (AHIC) is proposed to enhance the load adaptability. The AHIC utilizes a two-stage dc–ac–ac three-port converter, which has the following advantages:

1) This article addresses the failure of harmonic suppression in existing methods under load ripple current conditions. The proposed scheme improves load adaptability by independently controlling TPBR's injected current, which offers a new idea for advancing dc-side harmonic reduction methods.
2) The proposed AHIC can be implemented using a basic common converter, avoiding the special design and parameter dependence on auxiliary transformers in passive HRCs, unlike active HRCs, it transits from line-frequency to high-frequency isolation, achieving superior harmonic suppression with just one extra bridge arm.
3) The low voltage stress ($5\%U_{\rm dc}$) enables lightweight system design, resulting in a low VA rating ($2.5\%P_{\rm L}$) AHIC, adding less than 0.32% additional loss (prototype data). It also eliminates the bulky magnetic devices required by existing methods. The proposed scheme also has the merits of small size, low loss, and cost-effectiveness.
4) The proposed scheme does not need ac inductors, avoiding deterioration of dc voltage quality and power factor. Compared to the widely used APFs, the AHIC has a lower voltage level, smaller capacity, lower loss, and simpler control.
5) The proposed AHIC can be modularized and integrated into existing multipulse rectifiers to improve power quality.

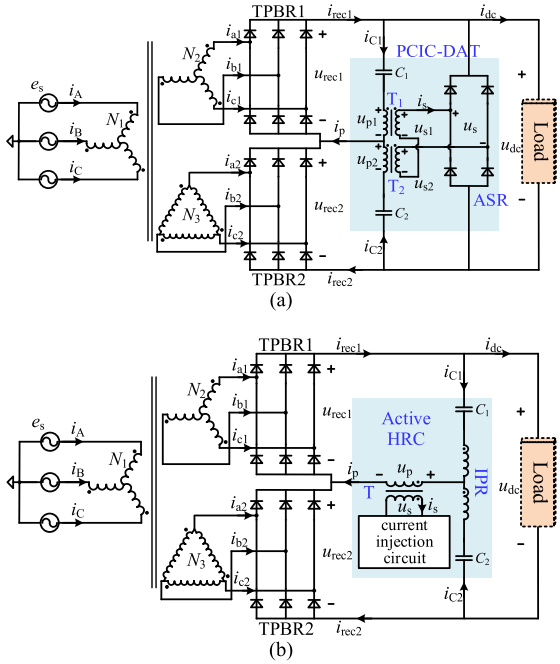

Fig. 1. Two typical circuits for DC side harmonic reduction methods. (a) 24-pulse rectifier with PCIC-DAT. (b) 12-pulse rectifier with active HRC.

II. Analysis of Load Adaptability

In this section, we analyze the load adaptability using representative dc side HRCs from two types of harmonic reduction methods [14], [19], as shown in Fig. 1. The harmonic suppression principle of the two circuits when the load current $i_{\rm dc}$ is a ripple-free constant value $I_{\rm dc}$ are shown in Figs. 2 and 3. Meanwhile, two nonideal load conditions are established based on the way and location of load current ripple generation. One

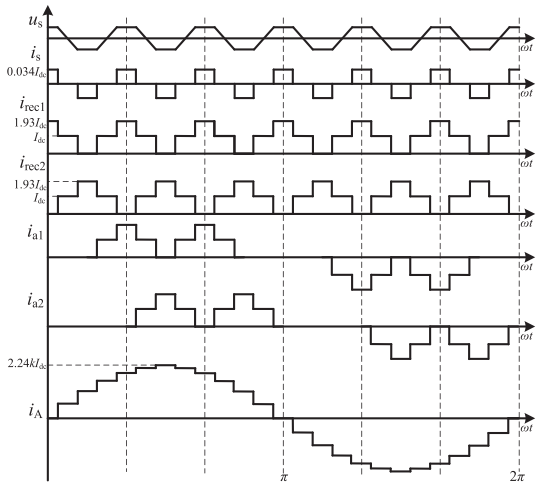

Fig. 2. Essential voltage and current waveforms of the 24-pulse rectifier with PCIC-DAT.

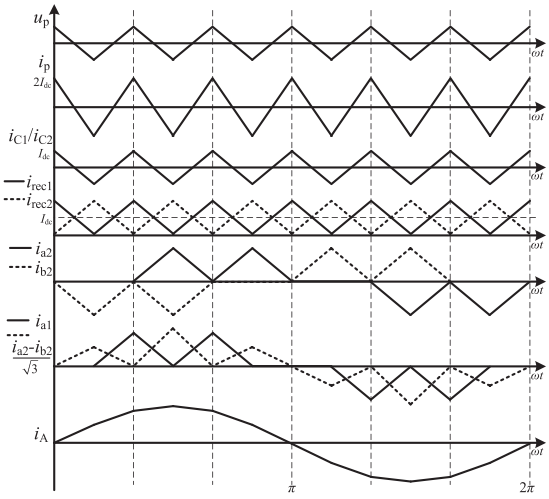

Fig. 3. Theoretical construction waveforms for input line current i_A of 12-pulse rectifier with active HRC.

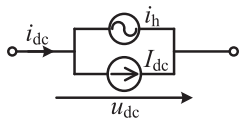

Fig. 4. Equivalent circuit for low-frequency pulsating current in load.

is the low-frequency pulsating current introduced by the load converter, arising from load side. The other is the harmonic current from TPBR's output caused by series resonance of the transformer leakage inductor and capacitive load, originating from the source side [34], [35], [36].

A. Harmonic Suppression Performance Under Low-Frequency Pulsating Load Current

The load converter generates a low-frequency pulsating input current, which cannot be fully decoupled by decoupling capacitors [35], [37]. The load can be equivalent to a dc current I_{dc} in parallel with a harmonic current i_h, as shown in Fig. 4. So, the

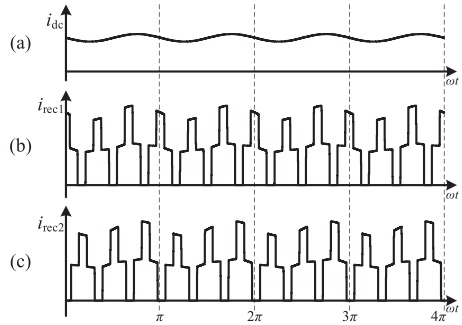

Fig. 5. Current waveforms of TPBR output in Fig. 1(a) with low-frequency pulsating current in load. (a) Load current i_{dc} of rectifier. (b) TPBR1 output current i_{rec1}. (c) TPBR2 output current i_{rec2}.

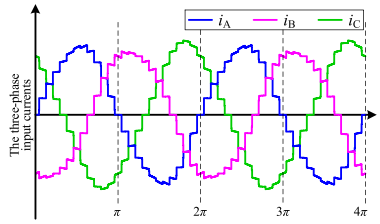

Fig. 6. Input line current waveforms of the rectifier in Fig. 1(a) under load current ripple.

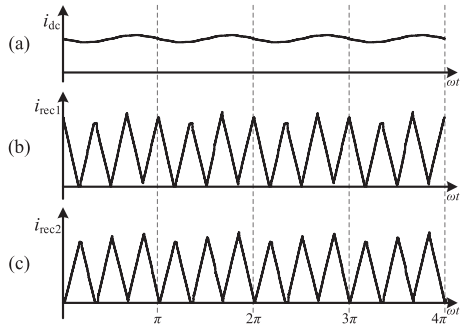

Fig. 7. Current waveforms of TPBR output in Fig. 1(b) with low-frequency pulsating current in load. (a) Load current i_{dc} of rectifier. (b) TPBR1 output current i_{rec1}. (c) TPBR2 output current i_{rec2}.

i_{dc} is expressed as

$$i_{dc} = I_{dc} + i_h. \tag{1}$$

Set the amplitude of i_h is $5\%I_{dc}$ and the frequency is 100 Hz (for 50 Hz grid). The load current and TPBRs output current waveforms for 24-pulse rectifier with PCIC-DAT are shown in Fig. 5. The harmonic current in i_{dc} is transmitted into two TPBRs, which causes i_{rec1} and i_{rec2} to overlap the undesired harmonic on original square-wave current. The three-phase input current waveforms are shown in Fig. 6, and Table I gives the main frequencies harmonic contents. It is observed that the 2nd pulsating current in dc side introduce the 3rd harmonic in ac current, which worsens the THDi from less than 5% to 9.5%, and the three-phase currents are unbalanced.

Similarly, the current waveforms for 12-pulse rectifier with active HRC are shown in Fig. 7. Also, Fig. 8 and Table I presents the three-phase input current waveforms and main frequency

TABLE I
HARMONIC CONTENTS OF THREE-PHASE INPUT CURRENT

Conditions/HRC		Harmonic	3rd (%)	5th (%)	7th (%)	11th (%)	13th (%)	23th (%)	25th (%)	THD (%)
1)	PCIC-DAT	i_A	5.07	—	—	—	—	4.37	3.86	8.86
		i_B	5.3	—	—	—	—	4.61	4.33	9.5
		i_C	4.85	—	—	—	—	3.59	3.59	8.21
	Active HRC	i_A	4.96	—	—	—	—	—	—	5.38
		i_B	5.22	—	—	—	—	—	—	5.61
		i_C	4.87	—	—	—	—	—	—	5.21
2)	PCIC-DAT	i_A	—	—	—	8.79	7.73	5.13	2.32	12.8
	Active HRC	i_C	—	2.43	2.19	11.5	10.3	—	—	16.12

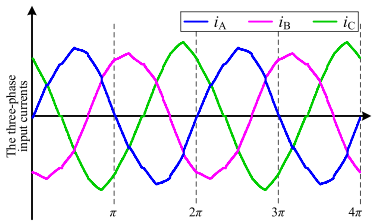

Fig. 8. Input line current waveforms of the rectifier in Fig. 1(b) under load current ripple.

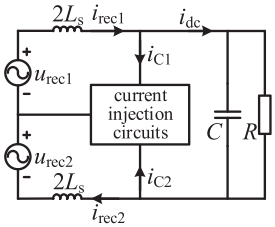

Fig. 9. Equivalent circuit for rectifier output loop generating series impedance resonance.

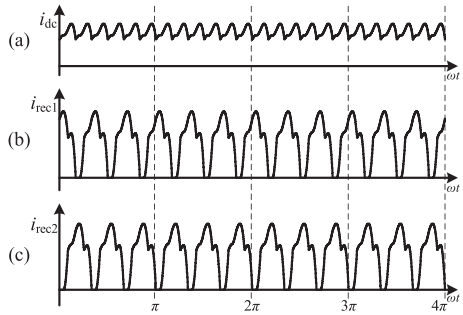

Fig. 10. Current waveforms of TPBR output in Fig. 1(a) with rectifier output series resonant current. (a) Series resonant current $i_{\rm dc}$. (b) TPBR1 output current $i_{\rm rec1}$. (c) TPBR2 output current $i_{\rm rec2}$.

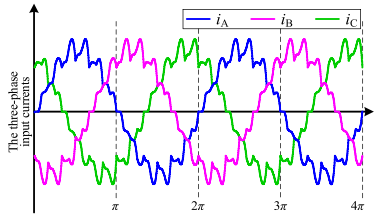

Fig. 11. Input line current waveforms of the rectifier in Fig. 1(a) under series impedance resonance.

harmonic contents. The low-frequency pulsating current of the load causes the deterioration of the input current THD from 1% to 5.61% and unbalance.

B. Harmonic Suppression Performance Under Series Resonant Load Current

When capacitors are parallel to a resistive load, the phase-shifting transformer's leakage inductor L_s will generate series resonance with the load capacitor C, causing harmonic current output from the TPBRs [34], [36]. The equivalent circuit is shown in Fig. 9. The harmonic current has the same frequency as the rectifier output ripple voltage, and its amplitude depends on the series resonant frequency and the load power [34].

The series resonant frequency is set to 205 Hz ($L_s = 150\ \mu$H and $C = 1000\ \mu$F). Since the injected circulating currents do not flow through the load side, the $i_{\rm dc}$ is the series resonant current from the rectifier output. Fig. 10 presents the load current and TPBRs output current waveforms for a 24-pulse rectifier with PCIC-DAT. It can be seen that the $i_{\rm dc}$ contains mostly 12th harmonic, causing severe distortions in expected square-wave of $i_{\rm rec1}$ and $i_{\rm rec2}$. So, the three-phase input current waveforms and main frequencies harmonic contents are shown in Fig. 11 and Table I. The 11th and 13th harmonic currents reappear and the THDi surges from less than 5% to 12.8%.

Also, the current waveforms for the 12-pulse rectifier with active HRC are shown in Fig. 12. The 12th harmonic is superimposed on the triangular current and changes the TPBRs output currents. The three-phase input current waveforms and main frequencies harmonic contents are shown in Fig. 13 and Table I. Apparently, the input current includes significant 11th and 13th harmonics, and its THD increases from 1% to 16.12%.

C. Mechanism of Poor Load Adaptability and Improvement Method

By analyzing the load adaptability of two methods, it is clear that the undesired harmonics in $i_{\rm dc}$ transmit to the TPBR output current, which worsens the input current THD. The dc side HRCs inject equal-amplitude and out-of-phase circulating currents into each TPBR output, i.e., $i_{C1} = i_{C2}$, to obtain desired shape

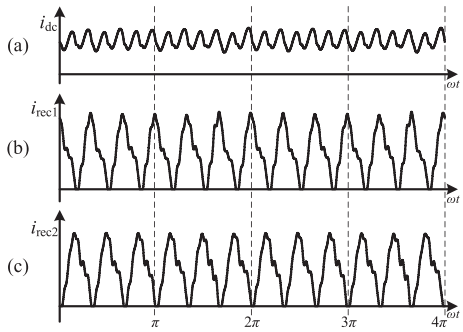

Fig. 12. Current waveforms of TPBR output in Fig. 1(b) with rectifier output series resonant current. (a) Series resonant current $i_{\rm dc}$. (b) TPBR1 output current $i_{\rm rec1}$. (c) TPBR2 output current $i_{\rm rec2}$.

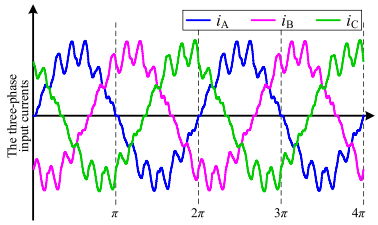

Fig. 13. Input line current waveforms of the rectifier in Fig. 1(b) under series impedance resonance.

$i_{\rm rec1\_ref}$ and $i_{\rm rec2\_ref}$ when $i_{\rm dc} = I_{\rm dc}$, which be expressed as

$$\begin{cases} i_{\rm rec1\_ref} = I_{\rm dc} + i_{C1} \\ i_{\rm rec2\_ref} = I_{\rm dc} - i_{C2} \end{cases}. \tag{2}$$

However, under the above-mentioned two typical load conditions, the $i_{\rm dc}$ includes harmonic current i_h, and then the rectifier output currents can be expressed as

$$\begin{cases} i_{\rm rec1} = I_{\rm dc} + i_h + i_{C1} \\ i_{\rm rec2} = I_{\rm dc} + i_h - i_{C2} \end{cases}. \tag{3}$$

Most dc side HRCs utilize magnetic devices to enforce $i_{\rm C1} = i_{\rm C2}$, which makes compensation i_h impossible. The failure to compensate for undesired currents i_h in $i_{\rm rec1}$ and $i_{\rm rec2}$ is the essential reason of poor load adaptability of available methods. If the injected currents $i_{\rm C1}$ and $i_{\rm C2}$ can be controlled independently, it offers the possibility of offsetting undesired harmonics, and improving load adaptability.

III. Proposed Rectifier and Operating Principle

A. Proposed Series-Connected 12-Pulse Rectifier With AHIC

The novel approach proposed in this article inserts two independent current sources in series with the capacitors C_1 and C_2 respectively to lower auxiliary circuit voltage level, as shown in Fig. 14. The two current sources (i_{C1} and i_{C2}) shape the applicable circulating current and compensate for the rectifier output undesired ripple currents, mitigating ac side harmonics under nonideal loads. It is worth mentioning that since i_{C1} and i_{C2} are independently controlled, there is no necessity to satisfy $i_{C1} = i_{C2}$, so the auxiliary circuit can remove the bulky magnetic devices (IPR and auxiliary transformer), improving the power density, efficiency, and cost of the rectifier.

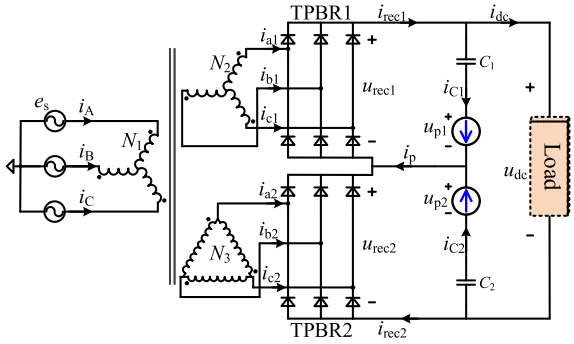

Fig. 14. Proposed method of independent current sources in series with C_1 and C_2.

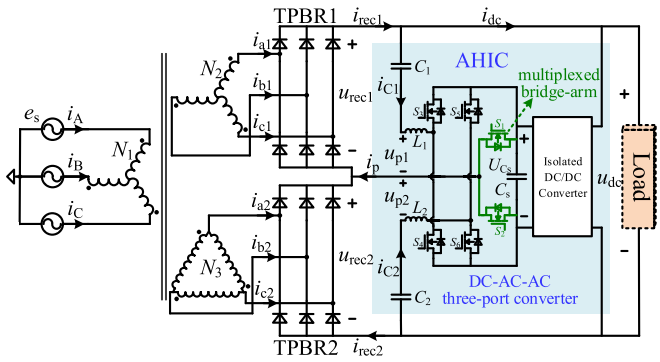

Fig. 15. Topology of proposed series-connected 12-pulse rectifier with AHIC formed by two-stage DC–AC–AC three-port converter.

In order to precisely obtain the required injection current, the current source can be realized with a two-stage auxiliary circuit which is the combination of a full-bridge PWM converter and dc/dc converter in [32] and [34], where isolated dc/dc converter ensure the necessary electrical isolation. However, using the same dc–ac topology for both current sources leads to an overly complex configuration that requires simplification. As two current sources have a common connection point, the two downstream full-bridge converters can multiplex one bridge-arm and retain one bridge-arm each to form a dc–ac–ac three-port converter. Also, the front-end isolated dc/dc converters can be simplified to one. The implementation of the two independent current sources in Fig. 14 is shown in Fig. 15.

The downstream dc–ac–ac three-port converter is used to precisely control the applicable injection currents i_{C1} and i_{C2}. From Fig. 15, the multiplexed bridge-arm output current is given by

$$i_p = i_{C1} + i_{C2}. \tag{4}$$

The front-end dc/dc converter employs DCX-LLC, which is connected with the load to provide stable intermediate voltage $U_{\rm Cs}$ and to feed active harmonic power to the load.

B. Operating Principle Under Ideal Load Condition

In an ideal load condition, the load current $i_{\rm dc}$ is a constant value $I_{\rm dc}$. The injected circulating currents $i_{C1} = i_{C2}$ are controlled as a realized symmetrical six times the main frequency

triangular wave with an amplitude of $I_{\rm dc}$, and an approximate sine ac input currents are obtained, as illustrated in Fig. 3.

Assume that the three-phase grid voltages are balanced, where phase voltage $e_A = E_p \sin(\omega t)$, E_p is the amplitude of e_s, $\omega = 2\pi f_{\rm o}$ is the fundamental angular frequency, and $f_{\rm o}$ is the fundamental frequency.

Define k is the ratio coefficient of the *Y*/*Y*/*D*1 phase-shifting transformer, and its winding turns ratio can be expressed as

$$N_1{:}N_2{:}N_3 = 1{:}k{:}\sqrt{3}k. \tag{5}$$

According to the construction of phase-shifting transformer and the operating principle of TPBRs, the Fourier series of $u_{\rm rec1}$ and $u_{\rm rec2}$ are as

$$\begin{cases} u_{\rm rec1} = U_{\rm rec1\_DC} + u_{\rm rec1\_AC} \\ \quad\quad = \frac{3\sqrt{3}}{\pi} kE_{\rm p} + \frac{6\sqrt{3}}{\pi} kE_{\rm p} \sum\limits_{n=1}^{\infty} \frac{-(-1)^n}{36n^2-1} \cos(6n\omega t) \\ u_{\rm rec2} = U_{\rm rec2\_DC} + u_{\rm rec2\_AC} \\ \quad\quad = \frac{3\sqrt{3}}{\pi} kE_{\rm p} + \frac{6\sqrt{3}}{\pi} kE_{\rm p} \sum\limits_{n=1}^{\infty} \frac{-(-1)^n}{36n^2-1} \cos\left[6\left(n\omega t + \frac{\pi}{6}\right)\right] \end{cases}. \tag{6}$$

The C_1 and C_2 in series with the AHIC are used to block the dc component in the rectifier bridges output voltages, so that their voltages are ideally expressed as

$$u_{C1} = u_{C2} = \left(3\sqrt{3}\Big/\pi\right) kE_p. \tag{7}$$

Further, the ac output voltages of the AHIC are as follows:

$$\begin{cases} u_{p1} = u_{\rm rec1\_AC} \\ u_{p2} = u_{\rm rec2\_AC} \\ u_p = u_{p1} - u_{p2} = \frac{3\sqrt{3}}{\pi} kE_p \sum\limits_{n=1}^{\infty} \frac{4}{36n^2-1} \sin\left(\frac{n\pi}{2}\right) \cos(6n\omega t). \end{cases} \tag{8}$$

It can be visualized that this unique structure helps reduce the voltage stress on the active components.

From Fig. 15 and (6), load voltage $u_{\rm dc}$ is calculated as

$$\begin{aligned} u_{\rm dc} &= u_{\rm rec1} + u_{\rm rec2} \\ &= U_{\rm dc}\left[1 + \sum_{n=1}^{\infty} \frac{2}{144n^2-1} \cos(n\pi)\cos(12n\omega t)\right] \end{aligned} \tag{9}$$

where the $U_{\rm dc}$ is the load average voltage, and it meets

$$U_{\rm dc} = \frac{6\sqrt{3}}{\pi} kE_p = 3.308kE_p. \tag{10}$$

According to the magnetomotive force equation of the phase-shifting transformer, the input currents on the primary side of the transformer are obtained as follows:

$$\begin{cases} i_{\rm A} = ki_{\rm a1} + \frac{k}{\sqrt{3}}(i_{\rm a2} - i_{\rm b2}) \\ i_{\rm B} = ki_{\rm b1} + \frac{k}{\sqrt{3}}(i_{\rm b2} - i_{\rm c2}) \\ i_{\rm C} = ki_{\rm c1} + \frac{k}{\sqrt{3}}(i_{\rm c2} - i_{\rm a2}) \end{cases}. \tag{11}$$

Under the ideal load condition, $i_{\rm rec1}$ and $i_{\rm rec2}$ can be obtained

$$\begin{cases} i_{\rm rec1} = I_{\rm dc} + i_{C1} \\ i_{\rm rec2} = I_{\rm dc} - i_{C2} \end{cases}. \tag{12}$$

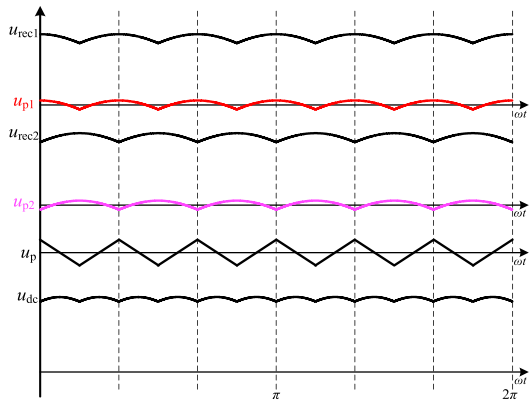

Fig. 16. Main voltage waveforms in continuous mode.

From Fig. 3, i_{C1} and i_{C2} are plotted as triangle and meet

$$i_{C1} = i_{C2} = I_{\rm dc} \sum_{n=1}^{\infty} \frac{8}{n^2\pi^2} \sin\left(\frac{n\pi}{2}\right) \cos(6n\omega t). \tag{13}$$

According to the operating principle of TPBRs, substituting (12) and (13) into (11), the Fourier series of i_A in Fig. 3 can be expressed as

$$\begin{aligned} i_A = \sum_{n=1}^{\infty} \frac{48}{n^2\pi^2} kI_{\rm dc} \sin\left(\frac{n\pi}{2}\right) \left[2\cos\left(\frac{n\pi}{6}\right) - \cos\left(\frac{n\pi}{3}\right) - 1\right] \\ \cdot \left[\sin(n\omega t) - \frac{2}{\sqrt{3}} \sin\left(\frac{n\pi}{3}\right) \cos\left(n\omega t + \frac{n\pi}{2}\right)\right]. \end{aligned} \tag{14}$$

From (14), it can be seen that the (12$n\pm$1)th (n is a positive integer) harmonics in input current are almost eliminated. The corresponding current waveforms are shown in Fig. 3, and the main voltage waveforms are shown in Fig. 16. Analyzing (6) and (13), both $u_{\rm rec}$ and $i_{\rm rec}$ contain 6nth ac components and the fundamental ac components of voltage and current are in phase for each six-pulse rectifier, as evident from Figs. 3 and 16. Thus, the AHIC absorbs active harmonic power from the input harmonic current.

C. Analysis of Harmonic Suppression Under Nonideal Load Conditions

The proposed AHIC possesses two degrees of freedom for circulating current control, contributing to the improvement of load adaptability. Under the nonideal load conditions, the rectifier output current before the circulating current is injected contains undesired harmonic components, which invalidates the harmonic suppression of the existing methods. By superimposing appropriate harmonics on triangular current to reshape the injected circulating current, the harmonic reduction effect of ac input current is achieved through ensuring, as much as possible, the TPBRs operate in critical continuous mode of Fig. 3.

1) Low-Frequency Pulsating Current: The equivalent circuit of 12-pulse rectifier with AHIC under low-frequency pulsating current is shown in Fig. 17. Considering the TPBRs conduct continuously, each 6-pulse rectifier can be represented by a dc and an ac sources in series ($U_{\rm rec\_DC}$ and $u_{\rm rec\_AC}$). The

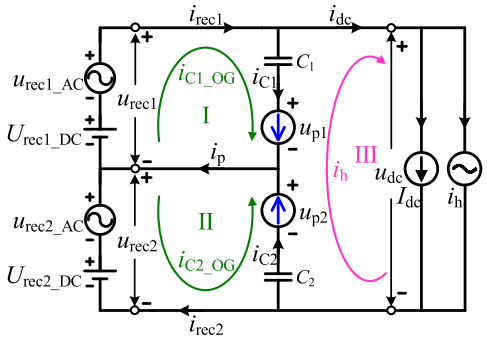

Fig. 17. Equivalent circuit of the 12-pulse rectifier with AHIC under low-frequency pulsating current.

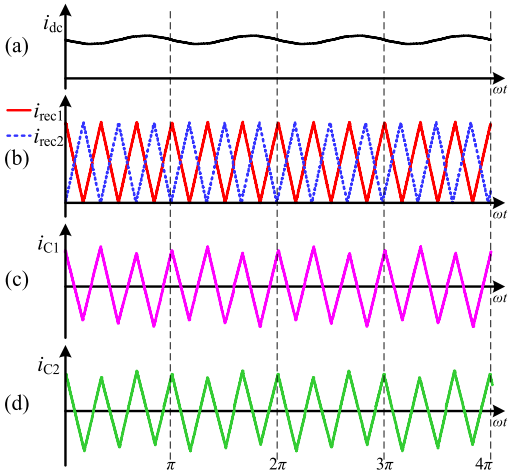

Fig. 18. Current waveforms of 12-pulse rectifier with AHIC in Fig. 15 with low-frequency pulsating load current. (a) Load current $i_{\rm dc}$. (b) TPBRs output current $i_{\rm rec1}$ and $i_{\rm rec2}$. (c) Injected circulating current $i_{\rm C1}$. (d) Injected circulating current i_{C2}.

low-frequency pulsating current i_h induces undesired harmonic current outputs from TPBRs, which worsens the input current THD, according to the analyzed results in Section II.

Combining (3) and Fig. 17, the injected circulating currents i_{C1} and i_{C2} must be reshaped to prevent i_h from affecting TPBR output waveform. Define the circulating currents under ideal load as $i_{\rm C1\_OG}$ and $i_{\rm C2\_OG}$ and the expression is (13). On this basis, i_{C1} should contain -i_h and i_{C2} should contain i_h, which ensures that $i_{\rm rec1}$ and $i_{\rm rec2}$ are ideal triangular currents as (2) and Fig. 3. So, two independent injection currents can be obtained

$$\begin{cases} i_{C1} = i_{\rm C1\_OG} - i_h \\ i_{C2} = i_{\rm C2\_OG} + i_h \end{cases}. \tag{15}$$

Analyzing the current flow from the inserted current sources in Fig. 17, first the original circulating current path I and path II remain unchanged, based on which two independent controlled current sources provide a load harmonic current path III. This avoids i_h flowing into the TPBRs outputs and improves its load adaptability.

The TPBRs output currents and AHIC injected circulating current waveforms under low-frequency pulsating load current are given in Fig. 18. Obviously, the load harmonic current i_h is superimposed on the triangular circulating current provided

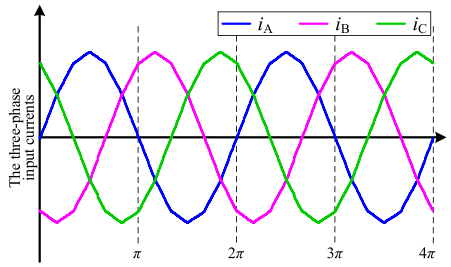

Fig. 19. Input line current waveforms of the rectifier in Fig. 15 under load current ripple.

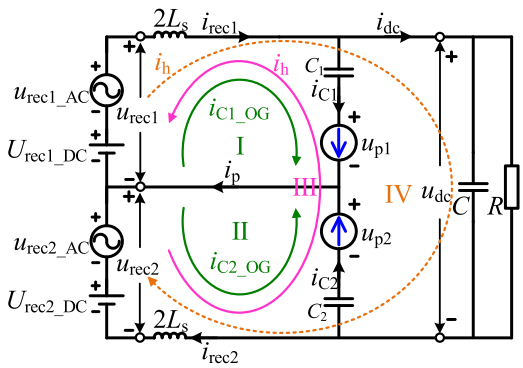

Fig. 20. Equivalent circuit of the 12-pulse rectifier with AHIC under resistive-capacitive load.

by the AHIC, which makes TPBRs output currents maintain the ideal triangle. Now, the three-phase input current waveforms are shown in Fig. 19, and its THD is only 1.28%.

2) Series Resonant Current: The equivalent circuit of a 12-pulse rectifier with AHIC under the resistive-capacitive load is shown in Fig. 20. The series loop impedance resonance leads to undesired harmonic current i_h in $i_{\rm rec1}$, $i_{\rm rec2}$, and $i_{\rm dc}$, causing the input current THD to increase dramatically. The series resonant current flows through the path IV as the dashed line in Fig. 20. It needs to be clarified that the series resonant current includes the dc load current $I_{\rm dc}$ and harmonic current i_h, and only i_h is labeled in Fig. 20 to illustrate the harmonic suppression mechanism of the AHIC.

The AHIC controls i_{C1} and i_{C2} to compensate the undesired harmonic current i_h in $i_{\rm rec1}$ and $i_{\rm rec2}$, whose compensation current flows through path III. Meanwhile, keeping the $i_{\rm C1\_OG}$ and $i_{\rm C2\_OG}$ fixed, the new injection currents still satisfy (15). Different from the load condition 1) in which AHIC provides a flow path for the load harmonic current to avoid i_h flowing into the TPBRs outputs, the compensation current from AHIC has two possible paths in the rectifier output series loop as shown in Fig. 21.

Ideally, the compensation current i_h should flow completely through path III-1 to offset the resonant current at the output of TPBRs. If i_h flows through path III-2, it will exacerbate the oscillation current on the load, which is not worth the cost. Therefore, an additional filter inductor L_f must be added to block the compensation current from entering the load side. It is apparent that L_f is larger than $2L_s$, ensuring the high-order harmonics will take the desired path. In addition, adding L_f lowers the

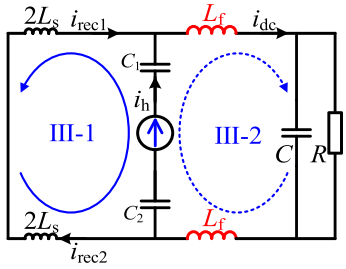

Fig. 21. Equivalent model of compensation current $i_{\rm h}$ flow paths.

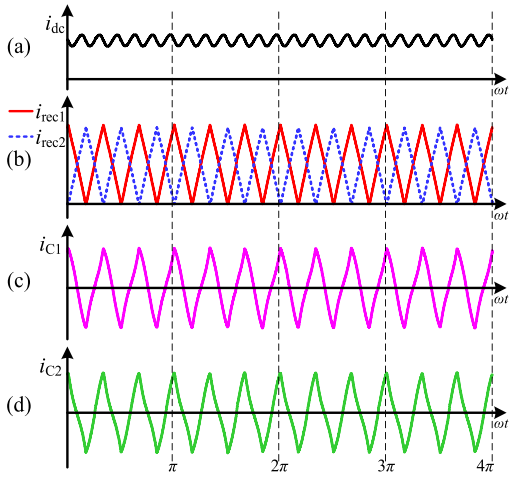

Fig. 22. Current waveforms of 12-pulse rectifier with AHIC in Fig. 15 with rectifier output series resonant current. (a) Series resonant current $i_{\rm dc}$. (b) TPBRs output current $i_{\rm rec1}$ and $i_{\rm rec2}$. (c) Injected circulating current $i_{\rm C1}$. (d) Injected circulating current $i_{\rm C2}$.

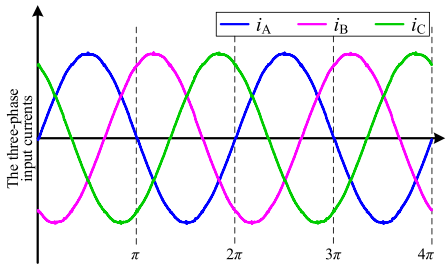

Fig. 23. Input line current waveforms of the rectifier in Fig. 15 under resistive-capacitive load.

series resonance frequency and suppresses the series impedance resonance. To decrease the passive filters, it is preferable to minimize the transformer leakage inductor L_s so that most of the compensation current takes the path III-1.

The TPBRs output currents and AHIC injected circulating current waveforms under series loop resonant current are plotted in Fig. 22. It is clear that the new injected circulating current is the original triangle plus compensating current i_h. The three-phase input current waveforms are shown in Fig. 23, with a THD of only 0.9%.

Summarily, the proposed 12-pulse rectifier with AHIC achieves the specific triangular currents output from TPBRs by compensating the undesired harmonic components in the original output current, thereby improving the harmonic reduction of ac input current under nonideal load.

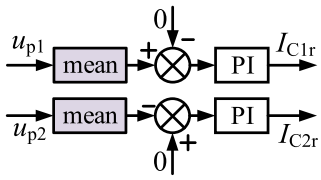

Fig. 24. Voltage balancing control link for capacitors C_1 and C_2.

D. Control Strategy

In the given case, a DCX-LLC resonant converter is used as the front-end of AHIC, which operates with a fixed switching frequency and does not require closed-loop control. The downstream dc–ac–ac three-port converter can be treated as a conventional PWM converter for output current control. The three-phase output currents of AHIC are transformed to $\alpha\beta$-frame, as follows:

$$\begin{bmatrix} i_\alpha \\ i_\beta \end{bmatrix} = \frac{2}{3}\begin{bmatrix} 1 & -\frac{1}{2} & -\frac{1}{2} \\ 0 & \frac{\sqrt{3}}{2} & -\frac{\sqrt{3}}{2} \end{bmatrix}\begin{bmatrix} -i_p \\ i_{C1} \\ i_{C2} \end{bmatrix}. \tag{16}$$

Control errors and component manufacturing variations can cause the voltages of C_1 and C_2 to deviate from the average output voltage of TPBR. This issue can be addressed by adding a small dc component to the current references of i_{C1} and i_{C2}, enabling voltage balancing. Fig. 24 shows the implementation of this control. By regulating the mean values of AHIC's port voltages u_{p1} and u_{p2} to 0, the current references $I_{\rm C1r}$ and $I_{\rm C2r}$ are generated and superimposed in (15).

According to (4) and (16), the reference currents in the $\alpha\beta$-frame for AHIC can be generated as

$$\begin{cases} i_{\alpha\_\rm ref} = -\left(i_{\rm C1\_OG} + i_{\rm C2\_OG} + I_{\rm C1r} + I_{\rm C2r}\right) \\ i_{\beta\_\rm ref} = -\frac{2}{\sqrt{3}} i_{\rm h} + \frac{1}{\sqrt{3}}\left(I_{\rm C1r} - I_{\rm C2r}\right) \end{cases}. \tag{17}$$

From Fig. 15, the AHIC output voltages in $\alpha\beta$-frame can be expressed as

$$\begin{bmatrix} u_\alpha \\ u_\beta \end{bmatrix} = \frac{1}{3}\cdot\frac{2}{3}\begin{bmatrix} 1 & -\frac{1}{2} & -\frac{1}{2} \\ 0 & \frac{\sqrt{3}}{2} & -\frac{\sqrt{3}}{2} \end{bmatrix}\begin{bmatrix} u_{p2}-u_{p1} \\ 2u_{p1}+u_{p2} \\ -2u_{p2}-u_{p1} \end{bmatrix}. \tag{18}$$

The above-mentioned equation is simplified as follows:

$$\begin{cases} u_\alpha = \frac{u_{p2}-u_{p1}}{3} \\ u_\beta = \frac{u_{p1}+u_{p2}}{\sqrt{3}} \end{cases}. \tag{19}$$

The control diagram of the system is shown in Fig. 25. In order to facilitate the generation of modulating waves for each bridge-arm, the current control is performed in $\alpha\beta$-frame. Analogous to existing current closed-loop control methods that track ac signals precisely, the current controller can adopt proportional quasi-resonant (PR) control or model predictive current control, etc., to obtain the required injected harmonic circulating current [36], [38], [39]. The PWM modulator can be used in bipolar modulation mode.

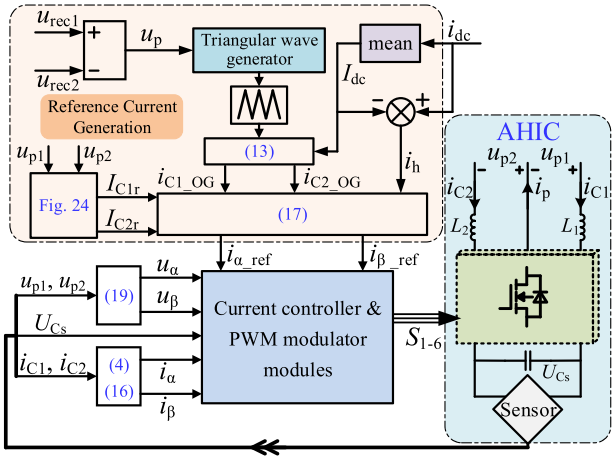

Fig. 25. Control system of the proposed AHIC.

The current references in $\alpha\beta$-frame i_{α_ref} and i_{β_ref} are made up of three components. The first component ensures that the tracking of the triangle reference. The desired triangular current reference i_{C1_OG} and i_{C2_OG} are generated by multiplying the load average current I_{dc} and the unit triangular wave, which is synchronized with the voltage difference u_p between u_{rec1} and u_{rec2}. The second component compensates for the undesired harmonic current i_h of the rectifier output. The i_h are extracted from i_{dc}, which contains the complete compensation current reference. However, when the series impedance has resonated, a small amount of compensation current is superimposed on the i_{dc} as a result of the shunt of the compensation current between path III-1 and path III-2 shown in Fig. 21. It is important to explain that extracting the harmonic current in i_{dc} at this point is still theoretically able to fully compensate for the undesired harmonic in i_{rec1} and i_{rec2}. The third part ensures that the AHIC output port voltages are pure ac, which will not affect harmonic suppression since I_{C1r} and I_{C2r} are small.

Assuming that the compensation current actually generated by the AHIC is i_{com}, the compensation current flows through path III-1 is λi_{com}, and then the compensation current flows through path III-2 is (1-λ)i_{com}, where λ is the compensation coefficient. The rectifier output currents before the AHIC input compensation are as follows:

$$i_{rec1} = i_{rec2} = i_{dc} = I_{dc} + i_h. \tag{20}$$

After the AHIC is put into compensation, the output currents of the TPBRs are expressed as (ignoring the injected triangular circulating current i_{C1_OG} and i_{C2_OG})

$$\begin{cases} i_{rec1} = i_{rec2} = I_{dc} + i_h - \lambda i_{com} \\ i_{dc} = I_{dc} + i_h + (1-\lambda)\, i_{com} \end{cases}. \tag{21}$$

Ideally, the current closed-loop control realizes zero steady-state error between the actual compensation current and the reference, i.e., it satisfies

$$i_{com} = i_h + (1-\lambda)\, i_{com}. \tag{22}$$

The above-mentioned equation can be simplified to obtain

$$\lambda i_{com} = i_h. \tag{23}$$

Substituting (23) into (21), the following can be obtained:

$$\begin{cases} i_{rec1} = i_{rec2} = I_{dc} \\ i_{dc} = I_{dc} + \frac{1}{\lambda} i_h \end{cases}. \tag{24}$$

From the above-mentioned equation, it can be seen that extracting the compensation current reference from i_{dc} is theoretically able to completely offset undesired harmonic current at the rectifier output. Unfortunately, the harmonics in load are amplified (because $0<\lambda<1$). Therefore, the transformer leakage inductor should be minimized and the L_f should be selected properly to prevent the load harmonics from being excessively large.

IV. Design of the AHIC

This section analyzes the specifications, main component sizing, and auxiliary circuit losses of the proposed AHIC, providing a reference for its implementation.

A. Component Sizing and Capacity of Active Circuit

On the basis of the compensation principle of AHIC, the injected circulating current superimposes the harmonic current from the i_{dc} on a specific triangular wave as in (15). In order to analyze the current stress on active devices, considering the worst condition, the harmonic current i_h is assumed as the same frequency and phase with the fundamental component in (13) and the amplitude is 10% of I_{dc}, which is expressed as

$$i_h = 0.1 I_{dc} \cos(6\omega t). \tag{25}$$

From (15), the root-mean-square (rms) and maximum values of i_{C2} can be determined as

$$\begin{cases} I_{C2\_rms} = 0.6476 I_{dc} \\ I_{C2\_max} = 1.1 I_{dc} \end{cases}. \tag{26}$$

Due to the circuit is symmetrical, the current stress of S_3–S_6 are same as (26). According to (4), the rms and maximum values of the multiplexed bridge-arm output current i_p is calculated as

$$\begin{cases} I_{p\_rms} = 1.1546 I_{dc} \\ I_{p\_max} = 2 I_{dc} \end{cases}. \tag{27}$$

The bridge-arm multiplexing technique reduces the number of active devices but also causes the current stress of S_1–S_2 to almost double.

According to (6) and (8), the rms and maximum values of the ac output port voltages for AHIC in continuous mode can be expressed as

$$\begin{cases} U_{p1\_rms} = U_{p2\_rms} = 0.0694 k E_p \approx 2.1\% U_{dc} \\ U_{(p1+p2)\_rms} = 0.034 k E_p \approx 1.03\% U_{dc} \end{cases}$$
$$\begin{cases} |u_{p1}|_{max} = |u_{p2}|_{max} = 0.154 k E_p \approx 4.66\% U_{dc} \\ |u_{(p1+p2)}|_{max} = 0.076 k E_p \approx 2.3\% U_{dc} \end{cases}. \tag{28}$$

Comparing with (10), the minimum value of U_{Cs} is $0.05U_{dc}$ for controllability. Considering an adequate voltage margin in practice, the U_{Cs} is set typically to about 7%–10% of U_{dc}.

Combining with (25), (27), and (28), the capacity of AHIC can be obtained as follows:

$$\begin{aligned} S_{\text{AHIC}} &= 0.5I_{p\_\text{rms}}\left(U_{p1\_\text{rms}}+U_{p2\_\text{rms}}\right)+I_{h\_\text{rms}}U_{(p1+p2)\_\text{rms}} \\ &= 0.0825kE_pI_{\text{dc}} \approx 2.5\%P_L \end{aligned} \tag{29}$$

where I_{h_rms} is the rms value of compensated harmonic current and P_L is the load power. Based on (8) and (13), the active power absorbed by AHIC in compensation process is

$$\begin{aligned} P_{\text{AHIC}} &= \frac{1}{T}\int_0^T \left[u_{p1}(t)-u_{p2}(t)\right]\cdot i_{C1}(t)dt \\ &= 0.07769kE_pI_{\text{dc}} \approx 2.35\%P_L. \end{aligned} \tag{30}$$

The VA rating of AHIC is only about 2.5% of load power, and due to the lower voltage level of downstream converter, the proposed active auxiliary circuit achieves partial power operation. Although the front-end DCX-LLC operates at a high voltage level, it only handles 2.35% of total load power.

The passive filters can be designed according to the typical procedure in the single-phase APF [40]. Since the quality of AHIC output compensation current directly affects the harmonic suppression performance of the rectifier, it is necessary to severely limit the inductor current ripple. The L_1 and L_2 can be obtained as follows:

$$L_1 = L_2 \geq \frac{U_{\text{Cs}}}{4\cdot\Delta I_{L\_\max} f_s} \tag{31}$$

where $\Delta I_{L\_\max}$ is max current ripple, take 5% of $I_{\text{C2\_max}}$ in the prototype design, and f_s is the switching frequency.

B. Size of Capacitors C_1 and C_2

The capacitors C_1 and C_2 block the dc voltage and extract the ripple component in the output voltages of TPBRs, which greatly reduces the AHIC output voltages level and minimizes the AHIC design capacity. In addition, it provides a good path for two independent controlled injection currents i_{C1} and i_{C2}.

As shown in Figs. 3 and 16, the fundamental voltage and current of the u_p and i_p are of the same frequency and phase. Therefore, the output of AHIC can be nearly equivalent to a resistor R_p, which with C_1 and C_2 make up a high-pass filter. The cut-OFF frequency satisfies

$$f_z = \frac{1}{2\pi R_p C_p} \tag{32}$$

where C_p, R_p, and f_z are the equivalent capacitor, equivalent resistor, and cut-OFF frequency of high-pass filter, respectively, and $C_p = C_1 = C_2$. The equivalent resistor R_p is the ratio of u_p and i_p fundamental amplitudes

$$R_p = \frac{U_{p\_6\omega}}{I_{p\_6\omega}}. \tag{33}$$

To provide a good injection current, the cut-OFF frequency of high-pass filter can only reach up to $6f_o$. By combining (32) and (33), if C_p is too small, the R_p will be increased to maintain the cutoff frequency of high-pass filter. Since i_p is generated by closed-loop control, it can be assumed that $I_{p\_6\omega}$ is constant, which will result in $U_{p\_6\omega}$ raising.

Considering the limitation of the dc voltage of the downstream converter, the f_z is set to (6/5)f_o. Substituting (8), (13), and (33) into (32), the values of C_1 and C_2 can be obtained as follows:

$$C_1 = C_2 \geq 3.77\frac{I_{\text{dc}}}{f_o U_{\text{dc}}}. \tag{34}$$

In addition, it is specified that the ripple voltage produced by the compensated current i_h flowing through C_1 and C_2 does not exceed 5% of U_{dc}, and C_1 and C_2 are also to be satisfy

$$C_1 = C_2 \geq 0.32\frac{I_{\text{dc}}}{h\cdot f_o U_{\text{dc}}} \tag{35}$$

where h is harmonic order of i_h. According to the constraints (34) and (35), the sizes of C_1 and C_2 can be determined.

C. Size of Additional Filter Inductor L_f

According to the harmonic suppression principle under the resistive-capacitive load, the compensation current i_h is split in two paths as shown in Fig. 21. Although it is theoretically possible to completely offset the undesired harmonics of the rectifier output by extracting the compensation current reference from the load current, the AHIC output currents and the load harmonic currents will increase significantly.

The λ is raised by adding additional filter inductor L_f on the load side to ensure that the compensation currents i_h flow into the design path as much as possible. At the series resonant frequency, the impedance of path III-2 is dominated by L_f, so the λ can be defined as follows:

$$\lambda = \frac{L_f}{2L_s + L_f}. \tag{36}$$

In order to minimize the AHIC design capacity, it is specified that the harmonic component in the i_{dc} does not increase by more than 1.1 times after the AHIC is put into compensation. Combining with (24), the value of the filter inductor L_f satisfies the following:

$$L_f \geq 20L_s. \tag{37}$$

According to (37), the additional filter inductor L_f is related to the phase-shifting transformer leakage inductor L_s. In order to minimize the capacity of the passive filter, it is preferable to lower the leakage inductor of transformer so that most of the compensation current flows through path III-1.

D. Analysis of Auxiliary Circuit Losses

The efficiency of the rectifier is a critical index in high-power applications. The loss ratio introduced by the AHIC determines its practical application value. The losses in the AHIC include switching device losses, capacitor losses, and inductor losses. Table II provides the calculation models for various types of losses. The component voltage and current stresses, as well as the rms and average current required for loss calculations, are listed in Table III. The front-end converter features stable U_{CS} and electrical isolation, offering a variety of circuit topology options. In this study, the DCX-LLC is selected as the prototype. To simplify the auxiliary circuit loss calculation, the loss of DCX-LLC are estimated based on a conservative average efficiency of

TABLE II
LOSS CALCULATION MODELS FOR MAIN COMPONENTS IN AHIC

Loss	Calculation model	Parameter
conduction	$P_{RS}=I_{SRMS}^2R_S$	R_s: on-resistance
switching	$P_{SS}=0.5V_SI_Sf_s(t_{on}+t_{off})$	t_{on}/t_{off}: switching times
capacitive	$P_{CS}=0.5V_S^2C_{oss}f_s$	C_{oss}: output capacitor
driving	$P_{GS}=V_{GS}Q_{GS}f_s$	V_{GS}: gate voltage Q_{GS}: gate charge
Total Switch	$P_S=P_{RS}+P_{SS}+P_{CS}+P_{GS}$	
copper	$P_{cu}=I_{LRMS}^2R_L$	R_L:AC resistance
iron	$P_{core}=\left(aB_{pk}^bf_S^c\right)A_el_e$	core material loss
Total Inductor	$P_{LL}=P_{cu}+P_{core}$	
capacitor	$P_C=I_{CRMS}^2R_C$	R_C: ESR

TABLE III
SPECIFICATIONS OF VOLTAGE AND CURRENT FOR MAIN COMPONENTS

Component	Voltage stress	Current stress	Current mean	Current rms
S_3–S_6	U_{Cs}	$1.1I_{dc}$	$0.282I_{dc}$	$0.4579I_{dc}$
S_1–S_2	U_{Cs}	$2I_{dc}$	$0.5I_{dc}$	$0.8164I_{dc}$
C_1/C_2	$0.5U_{dc}$	$1.1I_{dc}$	$0.59I_{dc}$	$0.6476I_{dc}$
L_1/L_2		$1.1I_{dc}$	$0.59I_{dc}$	$0.6476I_{dc}$

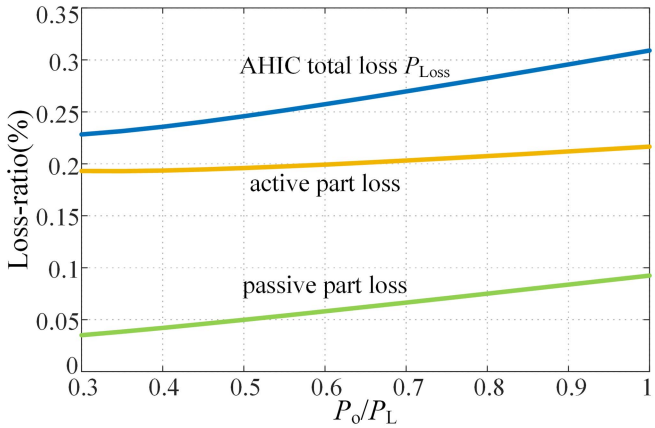

Fig. 26. Loss ratio of AHIC.

95%. Therefore, the total losses P_{Loss} introduced by the auxiliary circuit are as

$$P_{Loss}=P_{S12}+P_{S3-6}+P_{C12}+P_{LL12}+0.05P_{AHIC} \quad (38)$$

where P_{S12} represents the losses of switches S_1 and S_2, $P_{S3\text{-}6}$ is the losses of switches S_3–S_6, P_{C12} denotes the losses of capacitors C_1 and C_2, P_{LL12} is the losses of inductors L_1 and L_2, and the loss of DCX-LLC is 5% of P_{AHIC}.

Fig. 26 shows the loss ratio caused by AHIC to total system power based on the experimental prototype parameters, it is clear that the added AHIC has little effect on the efficiency advantage of the 12-pulse rectifier. This unique partial power design lowers the voltage level and the use of low-voltage MOSFETs with smaller on-resistance, thereby minimizing device losses and enhancing high-power rectifier performance.

V. COMPARISON WITH OTHER DC-SIDE HRCS AND EXPANSION OF AHIC

To clarify the strengths and weaknesses of the proposed scheme, the proposed AHIC is compared with other similar dc side HRCs, and its extended application examples are provided, with detailed results as follows.

A. Comparison With the 24-Pulse Rectifier Presented in [19]

Fig. 1(a) shows the 24-pulse rectifier with PCIC-DAT [19].

The PCIC-DAT contains two same auxiliary single-phase transformers (ASTs: T_1 and T_2) and auxiliary single-phase rectifier (ASR), which has the simplest design of magnetic devices among existing passive HRCs. By introducing additional rectifier operating modes and injecting square-wave currents into the TPBR outputs, the 12-pulse rectifier is extended to a new 24-pulse rectifier. The specific comparison results are given below:

1) The harmonic suppression of the circuit in Fig. 1(a) relies on the turns ratio of ASTs, which results in a fixed injected circulating current without active regulation capability. Under an ideal large inductive load, the optimal turns ratio design obtains an input current THD of 7.57%. But, under practical load ripple current conditions, its harmonic suppression will fail due to the inability to compensate for undesired harmonics in the TPBR outputs. In contrast, the proposed method offers flexible control over the injected circulating current, enabling effective suppression of input current harmonics under complex conditions.
2) Compared to the auxiliary circuits in [17] and [18], the PCIC-DAT requires one kind of magnetic device, simplifying its structure, with the ASTs designed for a capacity of 1.97% of load power. Since the ASR is connected in parallel with the load, the voltage stress across diode is u_{dc} , and the average current is $0.0085I_{dc}$. In addition, the filter capacitor parameters affect the quality of the injected circulating current, making large capacitors essential for harmonic suppression. The proposed AHIC removes the magnetic devices, with a slightly higher design capacity of 2.5% of load power due to its better harmonic suppression performance. Compared to passive HRCs, the proposed scheme requires additional control, driving, and sampling circuits, which increases system design complexity. To address this, the AHIC topology is simplified using switch-multiplexing technology, which is implemented by a simple and common converter. In practical applications, since AHIC has no special design requirements, commercially available mature products can be integrated into multipulse rectifiers for harmonic suppression. So, the AHIC is relatively easy to implement and cost-effective to control. The C_1 and C_2 branch currents are directly controlled by the AHIC, and their parameters affect the AHIC voltage level but do not impact the quality of the injected circulating current. The capacitors are selected by

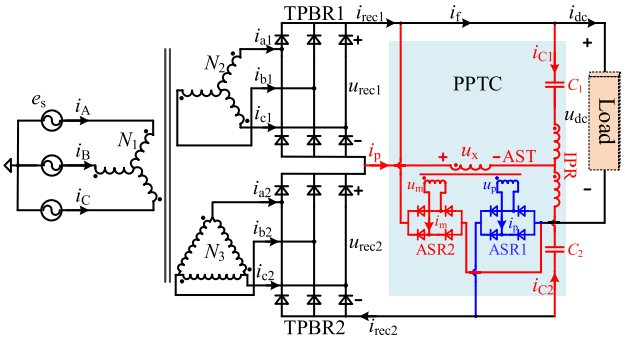

Fig. 27. 36-pulse rectifier with PPCT on the DC side.

considering the tradeoff between AHIC voltage stress and passive component capacity.

3) System efficiency is evaluated by comparing the loss ratio of auxiliary circuits under identical power and voltage ratings. In Fig. 1(a), the auxiliary circuit losses originate from the filter capacitors, ASTs, and ASR. To simplify the analysis, the AST loss are estimated based on a 98% efficiency standard. The loss ratio of PCIC-DAT is about 0.2%, which is better than that of the AHIC (0.32%). This is because the efficiency of the active circuit is obviously not up to the level of 98%. In future applications, selecting higher-quality switching devices could further enhance the efficiency of the active circuit.

B. Comparison With the 36-Pulse Rectifier Presented in [20]

Fig. 27 shows the 36-pulse rectifier with passive pulse-tripling circuit (PPTC) on the dc side [20].

The PPTC combines a series-type SCIPAC in [15] with a parallel-type SCIPAC in [17]. Composite modulation of the two ASRs increases the pulse number of the rectifier from 12 to 36. By optimizing the two turns ratio of AST, the input current THD is reduced to 5.04% under ideal conditions. Due to the different connection methods of ASR1 and ASR2, the two sets of turns ratios of AST vary significantly, increasing the complexity of magnetic device manufacturing. While AST and IPR are completely different magnetic devices operating at different voltage frequencies, which not only increases the difficulty of PPTC design but also brings obstacles to the optimal design of the rectifier [19].

Based on the rectifier operating principle under the optimal turns ratio of the AST, the AST is designed for a capacity of 2.3% of load power, while the IPR is designed for about 0.04% of load power, and the total capacity of the magnetic devices amounts to 2.34% of load power. In addition, the rms value of current through the diode in ASR1 is $0.7I_{\mathrm{dc}}$, and the rms value of current through the diode in ASR2 is $0.012I_{\mathrm{dc}}$. Using the same loss calculation model as the PCIC-DAT, the additional loss ratio introduced by PPTC account for 1.3%, which is primarily due to the significant diode conduction losses caused by the series connection of ASR1 with the load.

Compared to the proposed AHIC, the PPTC utilizes only passive components, offering a simpler structure. However, its harmonic suppression performance heavily relies on device parameters without the flexibility to control the injected circulating current, and the additional losses caused by the auxiliary circuit are relatively high.

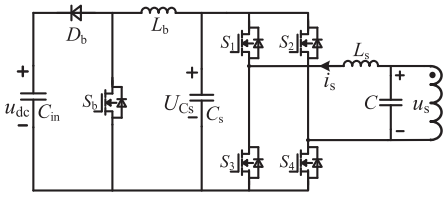

Fig. 28. Two-stage auxiliary circuit proposed in [32].

C. Comparison With the 12-Pulse Rectifier Based on Active HRC Presented in [14]

Fig. 1(b) shows the 12-pulse rectifier with active HRC [14].

The active HRC consists of an AST (T) and an active converter connected with the secondary side of T. By indirectly controlling the injected circulating current i_p as a specific triangle and equalizing it to the two TPBR outputs using the IPR, the input currents can be modulated to near-sinusoidal waves. The current injection circuit can be any active circuit that can output the required current. Fukuda et al. [31] employ a full-bridge converter to achieve triangular current injection, with its input connected to C_1 or C_2 and its output linked to the secondary side of T. However, this structure results in high voltage stress on the active components and a large turns ratio for AST, leading to poor control precision of the injected circulating current. To address this, [32] proposes a two-stage dc/ac circuit, as shown in Fig. 28, which utilizes a front-end boost converter to reduce the voltage level of the downstream PWM converter. This topology design allows for a reasonable turns ratio of AST, enabling effective control of the triangular current.

1) The active HRC features one degree of freedom for injected circulating current control. By using auxiliary magnetic devices to inject identical circulating currents into the TPBR outputs, the input current THD is reduced to just 1% when the load current is constant. However, based on the analysis in Section II, its harmonic suppression fails under nonideal load conditions due to the inability to compensate for undesired harmonics in the rectifier output.

2) Comparing the auxiliary circuit structures in Figs. 15 and 28, the proposed AHIC converts the low-frequency isolation transformer into a high-frequency isolated dc/dc converter and eliminates the IPR used for circulating current distribution, reducing magnetic component losses and device size and weight. The three-phase PWM converter in this article replaces the single-phase PWM converter in [32] by adding only one additional bridge arm and one filter inductor, and enables independent control of the injected circulating currents for both TPBRs, which doubles the degree of freedom of the current control, and significantly improves the input current harmonic suppression effect under nonideal load conditions. So the proposed method offers greater practicality.

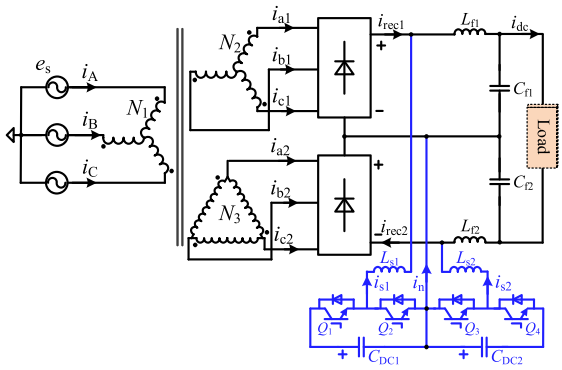

Fig. 29. Configuration of the 12-pulse rectifier with current sources formed by two buck-boost converters.

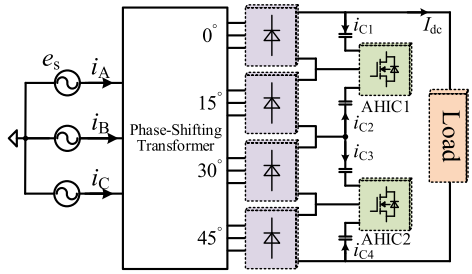

Fig. 30. Novel rectifier topology is derived from the proposed AHIC extended to the 24-pulse rectifier.

3) The magnetic device capacity of active HRC is 2.64% (AST: 2.34%, IPR: 0.3%) of load power. The voltage stress of the PWM rectifier is $7\%U_{\rm dc}$, and the rms value of the current flowing through S_1–S_4 is $0.8164I_{\rm dc}$. Based on the auxiliary circuit loss calculation model established in this article, under the same system specifications, the additional losses caused by the auxiliary circuit in Figs. 1(b) and 28 account for 0.4%, slightly higher than those of the proposed AHIC.

D. Comparison With the 12-Pulse Rectifier Based on Two Cascaded Buck-Boost Converters Presented in [30]

Fig. 29 shows the 12-pulse rectifier with two cascaded buck-boost converters [30].

An approach proposed in [30] inserts two current sources into the 12-pulse rectifier. The two current sources (i_{s1} and i_{s2}) in parallel with each rectifier are used to shape the TPBRs output currents $i_{\rm rec1}$ and $i_{\rm rec2}$ in order to suppress ac side harmonics. To reduce the VA rating of the active circuit (i.e., minimize the rms of compensation current), the parameters of rectifier output *LC* filter are optimized to ensure that the *LC* filter is purely resistive at the frequency of $6f_{\rm o}$. While the ESR of *LC* filter is carefully selected to shape the rectifier output current as closely as possible to the desired triangle. As a result, the auxiliary current source only needs to compensate for the differential current, significantly reducing its VA rating.

1) The approach in Fig. 29, similar to the proposed AHIC, is capable of independently controlling the injected circulating currents for both TPBRs, which has good load adaptability and is able to achieve input current harmonic suppression under complex operating conditions.
2) The current sources in Fig. 29 are connected in parallel with rectifier output. Since the output voltage is unipolar, a half-bridge circuit suffices for independent current control. In contrast, the proposed AHIC requires a full-bridge circuit for its current source implementation as the ac output voltage, resulting in an extra bridge arm compared to the auxiliary circuit in Fig. 29. Note that the front-end converter has been omitted in Fig. 29, which is essential for the dc side active harmonic reduction methods. The proposed AHIC connects the current source in series with the filter capacitor and then inserted into TPBR output. This configuration significantly reduces the voltage rating of AHIC ($5\%U_{\rm dc}$) compared to the converter (about $50\%U_{\rm dc}$) in Fig. 29, which facilitates light-weight design of active circuit and reducing switching losses by selecting high-performance, low-voltage devices.
3) The design capacity of the auxiliary circuit in Fig. 29 depends on the resonant frequency and ESR of the *LC* filter, which undoubtedly increases manufacturing complexity and cost in practical applications. Moreover, the optimal ESR varies with the load resistance, leading to a design capacity of the active circuit reaching 14% of load power. In the provided design example, the rms value of i_{s1} is about 20% of $I_{\rm dc}$. Under the same system specifications, the additional losses introduced by the auxiliary circuit in Fig. 29 account for about 2.3%, mainly the conduction losses of the ESR, which is much higher than the 0.32% loss ratio of the AHIC.

Table IV gives the comparison results between the proposed 12-pulse rectifier with AHIC and the above-mentioned four rectifiers. Compared to passive HRCs, the proposed AHIC, despite its more complex circuit implementation, utilizes a common topology that requires no special design, which can achieve input current harmonic suppression under complex conditions using modular products. Compared to active HRCs, although an additional bridge arm is added, the AHIC eliminates the AST and IPR, significantly reducing the voltage stress and design capacity of the auxiliary circuit. This results in greater load adaptability, lower losses and cost, and simpler implementation.

Table V gives the comparison results between the proposed 12-pulse rectifier with AHIC and APF and Vienna rectifier. In high-power rectification applications, the multipulse rectifiers based on dc-side AHIC can meet grid harmonic requirements with lower cost, smaller size and weight, higher efficiency, simpler control, and longer lifetime. However, the proposed diode rectifier cannot regulate the output voltage.

E. Expansion to Series-Connected 24-Pulse Rectifier

The proposed AHIC can be extended to series-connected 24-pulse rectifier to further improve its input current THD and the circuit structure is shown in Fig. 30.

The phase-shifting transformer outputs four line voltages with a phase difference of 15° as the input voltages of the four sets TPBRs, and two AHICs are inserted into the dc side to

TABLE IV
COMPARISON WITH SIMILAR DC-SIDE HARMONIC REDUCTION METHODS FOR 12-PULSE RECTIFIERS

Indicators		24-pulse rectifier with PCIC-DAT proposed in [19] [see Fig. 1(a)]	36-pulse rectifier with PPTC proposed in [20] [see Fig. 27]	12-pulse rectifier with active HRC proposed in [14] [see Fig. 1(b) and Fig. 28]	12-pulse rectifier with two current sources proposed in [30] [see Fig. 29]	Proposed 12-pulse rectifier with AHIC (see Fig. 15)
Auxiliary circuit type		Passive HRC	Passive HRC	Active HRC	Active HRC	Active HRC
Harmonic reduction method		harmonic injection	harmonic injection	output current modulation	output current modulation	output current modulation
AC harmonic suppression effect(THD)		ideal load: 7.6% nonideal: bad	ideal load: 5.1% nonideal: bad	ideal load: 1% nonideal: bad	ideal load: 1% nonideal: good	ideal load: 1% nonideal: good
Load adaptability/Independent current control		Poor/no	Poor/no	Poor/yes(1)	Robust/yes(2)	Robust/yes(2)
Auxiliary circuit structure		simple	relatively simple	complex	complex	common
Loss ratio of auxiliary circuit		0.2%P_{L}	1.3%P_{L}	0.4%P_{L}	2.3%P_{L}	0.32%P_{L}
Number of HRC components	AST	2	1	1	0	0
	IPR	0	1	1	0	0
	Diode	4	8	0	0	0
	MOSFET or IGBT	0	0	4	4	6
	Front-end converter	0	0	Boost	Isolated DC/DC	DCX-LLC
	Capacitor	2	2	2	2	2
	Inductor	0	0	1	4	2
AST	Magnetic ratings	1.97%P_L	2.3%P_L	2.34%P_L	–	–
	Structure	conventional	two secondary winding	conventional	–	–
	Turns ratio requirement	28.35	42.98/0.653	1	–	–
IPR	Magnetic ratings	–	0.04%P_L	0.3%P_L	–	–
Overall magnetic ratings		1.97%P_L	2.34%P_L	2.64%P_L	–	–
Auxiliary diodes	Voltage stress	U_{dc}	$U_{\mathrm{dc}}(4)$	–	–	–
	Current stress	0.034I_{dc}	$I_{\mathrm{dc}}(4)$ 0.031$I_{\mathrm{dc}}(4)$	–	–	–
	Current rms value	0.0085I_{dc}	0.99$I_{\mathrm{dc}}(4)$ 0.018$I_{\mathrm{dc}}(4)$	–	–	–
Active HRC/ switching device	Design capacity	–	–	2.34%P_L	14%P_L	2.5%P_L
	Voltage stress	–	–	0.07U_{dc}	0.5U_{dc}	0.05U_{dc}
	Current stress	–	–	2I_{dc}	0.28I_{dc}	1.1$I_{\mathrm{dc}}(4)$ 2$I_{\mathrm{dc}}(2)$
	Current rms value	–	–	0.8164I_{dc}	0.1414I_{dc}	0.4579$I_{\mathrm{dc}}(4)$ 0.8164$I_{\mathrm{dc}}(2)$
	Current mean value	–	–	0.5I_{dc}	0.1273I_{dc}	0.282$I_{\mathrm{dc}}(4)$ 0.5$I_{\mathrm{dc}}(2)$
Filter capacitors C_1 and C_2	Voltage stress	0.5U_{dc}	0.5U_{dc}	0.5U_{dc}	0.5U_{dc}	0.5U_{dc}
	Current rms value	0.683I_{dc}	0.62I_{dc}	0.5773I_{dc}	0.5445I_{dc}	0.6476I_{dc}
	Effect on THD	yes	yes	no	yes	no
Filter inductor	Current rms value	–	–	1.1546I_{dc}	0.2$I_{\mathrm{dc}}(2)$ 1.5445$I_{\mathrm{dc}}(2)$	0.6476I_{dc}
Cost		low	medium	high	high	controllable
Dependence of THD on component parameters		high	high	high	high	low
Prospects for practical applications		limited	limited	limited	low	high

control the injected circulating currents of the four sets TPBRs, respectively. The shapes of the injected circulating currents are determined based on the voltage difference between the outputs of adjacent rectifiers. As a result, a triangular current with the amplitude of I_{dc} and the frequency of $12f_{\mathrm{o}}$ is generated, and $i_{C1} = i_{C2} = i_{C3} = i_{C4}$. The simulation results in Fig. 31 are obtained. The results show that before the AHICs output the circulating currents, the input current THD of the 24-pulse rectifier is 7.55%. After AHICs inject the specific triangular circulating current, the input current THD of the 24-pulse rectifier is reduced

TABLE V
COMPARISON RESULTS OF THREE HARMONIC SUPPRESSION STRATEGIES

Type	Proposed DC side AHIC	AC side APF	Vienna rectifier
Input current THD	low	low	low
Active part capacity	low	medium	high
Cost	low	medium	high
efficiency	high	medium	low
Volume and weight	low	medium	high
Control complexity	simple	complex	medium
Lifetime	long	medium	short

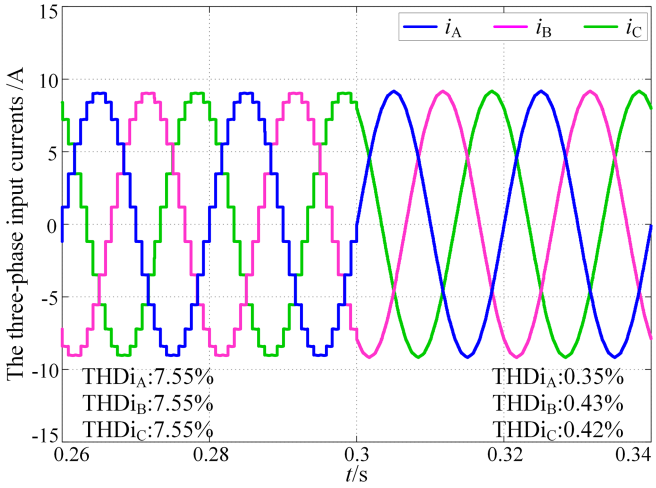

Fig. 31. Input line current waveforms of the rectifier in Fig. 30 under constant load current.

to below 0.5%. This demonstrates that the proposed AHIC is also applicable to series-connected 24-pulse rectifiers, significantly reducing the input current THD. In the future, we will continue to explore a general design method for applying the proposed AHIC to any multipulse rectifiers.

VI. EXPERIMENTAL VERIFICATION

In order to verify the feasibility of the proposed series-connected 12-pulse rectifier with AHIC, and to compare the harmonic suppression with the existing dc side active HRC under different load conditions. A 2-kW experimental prototype referring to Fig. 15 is built as shown in Fig. 32. Table VI gives the prototype design specifications. This experimental platform is also used to simulate the 12-pulse rectifier with active HRC shown in Fig. 1(b), which can only inject the specific triangular circulating current.

Condition I: Under the ideal large inductive load, the load current i_{dc} approximated as a dc current. Fig. 33 shows the experimental waveforms of the 12-pulse rectifier without HRC. The rectifier input current exhibits a 12-step current with THD of 11.5%. When the AHIC is employed, the experimental waveforms of the input current i_A and the injected circulating current i_{C1} and i_{C2} are shown in Fig. 34. Obviously, the input current waveform is close to sinusoidal and its THD is reduced to 2.25%, which means that dc side active HRCs have significant

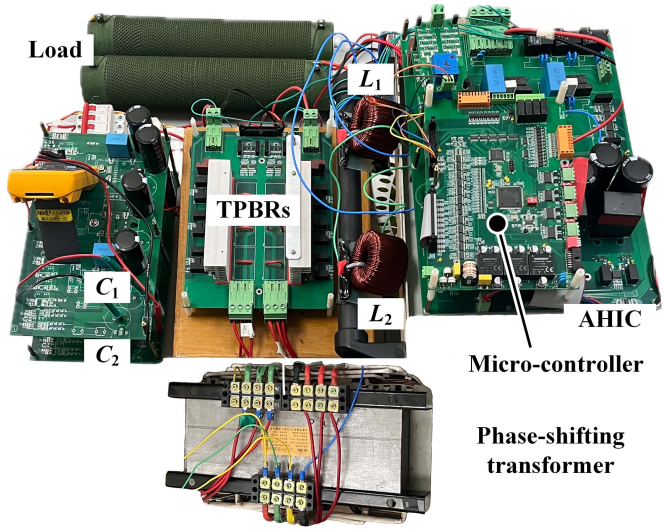

Fig. 32. Experimental prototype of the 12-pulse rectifier with AHIC.

TABLE VI
SPECIFICATIONS AND PARAMETERS OF THE 12-PULSE RECTIFIER WITH AHIC

	Parameters	Values
system	Source voltage $e_{s(RMS)}$	110 V
	Fundamental frequency f_o	50 Hz
	DC bus voltage U_{dc}	410 V
	Power rating P_L	2000 W
	Ratio coefficient of transformer k	0.8
	Leakage inductor L_s	100 μH
AHIC	Switching frequency f_s	50 kHz
	Intermediate DC voltage U_{Cs}	50 V
	Filter inductors (L_1,L_2)	800 μH
	Filter capacitors (C_1,C_2)	2.24 mF
	Filter inductor L_f	3 mH
	Intermediate DC capacitor C_s	500 μF
DCX-LLC	Switching frequency	200 kHz
	Turns-ratio	8:1

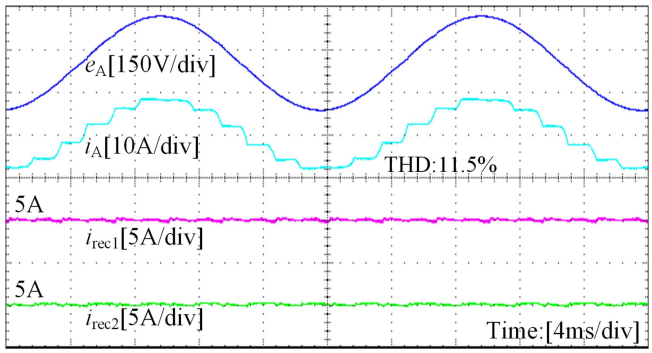

Fig. 33. Experimental waveforms of the 12-pulse rectifier without HRC in condition I.

input current harmonic suppression capability under ideal load conditions. Fig. 35 presents the i_A harmonic spectrum of the proposed rectifier at 100% and 20% rated power. It is obvious that under both full-load and light-load conditions, the THD meets the requirements of the IEEE-519 standard.

Condition II: When the load current i_{dc} contains low-frequency pulsating currents (10%I_{dc}, 100 Hz), the current waveforms of a 12-pulse rectifier without HRC are shown in

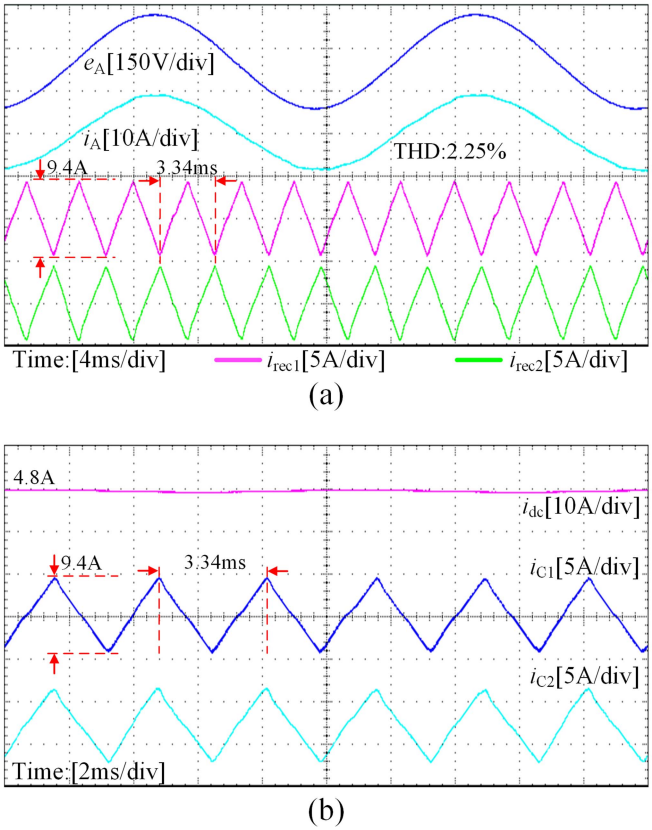

Fig. 34. Experimental waveforms of the 12-pulse rectifier with AHIC in condition I. (a) Input and output current waveforms of 12 pulse rectifier. (b) Load current i_{dc} and AHIC injection current i_{C1} and i_{C2}.

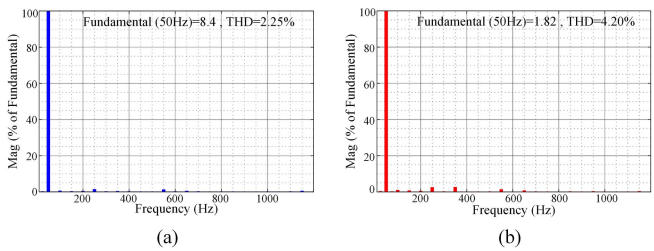

Fig. 35. Input current spectrum of the proposed rectifier in condition I. (a) 100%P_{L}. (b) 20%P_{L}.

Fig. 36, and the THD of input current i_A is 11.8%. Fig. 37 shows the experimental waveforms of the existing 12-pulse rectifier with active HRC as Fig. 1(b). Since the active HRC injects only specific triangular currents as shown in Fig. 37(b), this results in TPBRs output currents having undesired harmonic of i_{dc}, which makes the THD of i_A to be 6.65%. Fig. 38 illustrates the experimental waveforms of the proposed 12-pulse rectifier with AHIC. The injected current contains undesired harmonics of i_{dc} and the TPBRs output currents are the desired triangle, which ensures the THD of i_A low as 2.38%. Fig. 39 presents the i_A harmonic spectrum of the proposed rectifier at 100% and 20% rated power, and the THD meets the IEEE-519 standard.

Condition III: Under the resistive-capacitive load, series impedance resonance occurs in the rectifier output loop. The

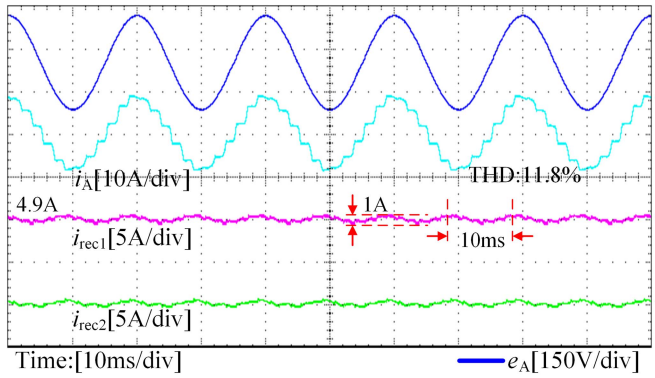

Fig. 36. Experimental waveforms of the 12-pulse rectifier without HRC in condition II.

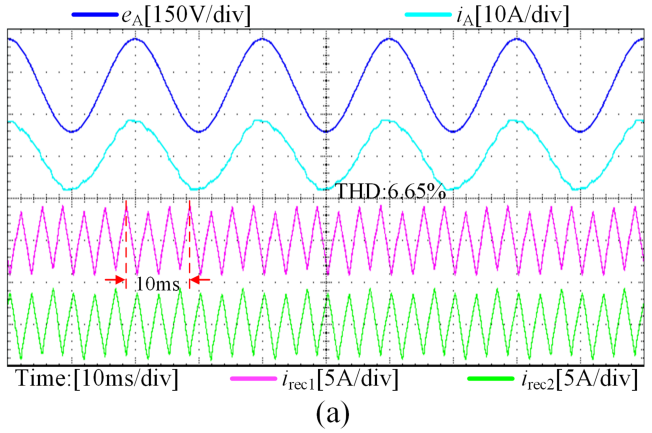

Fig. 37. Experimental waveforms of existing 12-pulse rectifier with active HRC in condition II. (a) Input and output current waveforms of 12 pulse rectifier. (b) Load current i_{dc} and AHIC injection current i_{C1} and i_{C2}.

series resonant current (15%I_{dc}) affects the TPBRs output current waveforms, causing distortion of the rectifier input current. Fig. 40 shows the experimental waveforms of the 12-pulse rectifier without HRC, and the THD of i_A is 13.5%. Fig. 41 displays the experimental waveforms of the existing 12-pulse rectifier with active HRC. Due to the lack of compensation for series loop resonance current in the TPBRs output, the THD of i_A up to 8.1%. Fig. 42 shows the experimental waveforms of the proposed 12-pulse rectifier with AHIC. The injected current contains a series resonance current in the TPBRs output, ensuring a low THD of 2.51% for the i_A. Fig. 43 presents the i_A

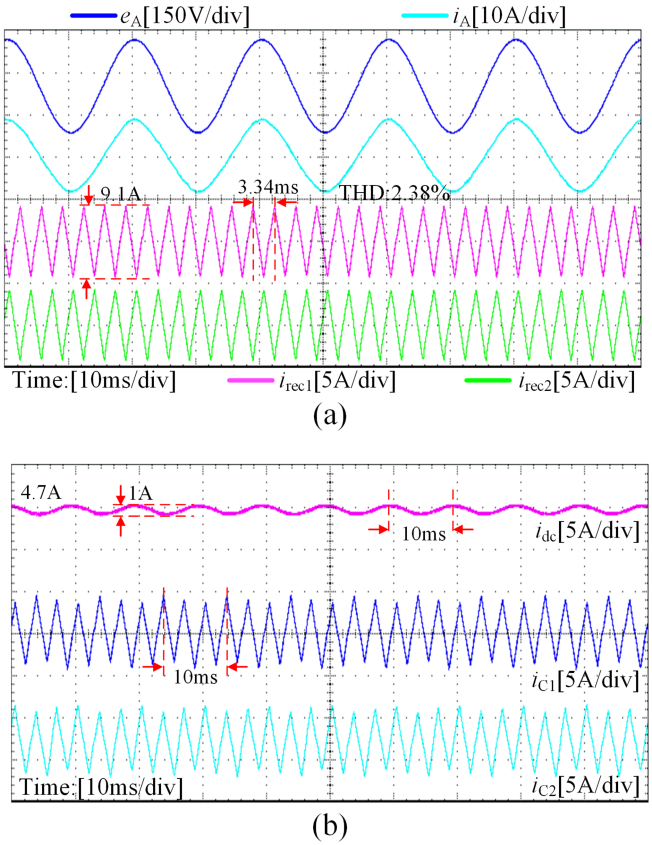

Fig. 38. Experimental waveforms of proposed 12-pulse rectifier with AHIC in condition II. (a) Input and output current waveforms of 12 pulse rectifier. (b) Load current $i_{\rm dc}$ and AHIC injection current i_{C1} and i_{C2}.

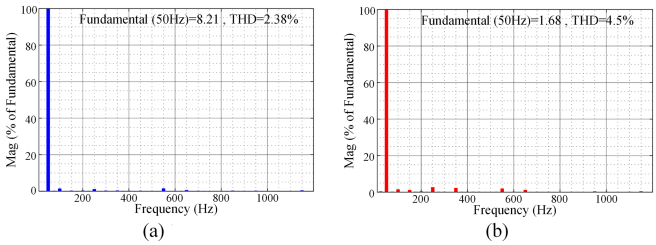

Fig. 39. Input current spectrum of the proposed rectifier in condition II. (a) 100%P_L. (b) 20%P_L.

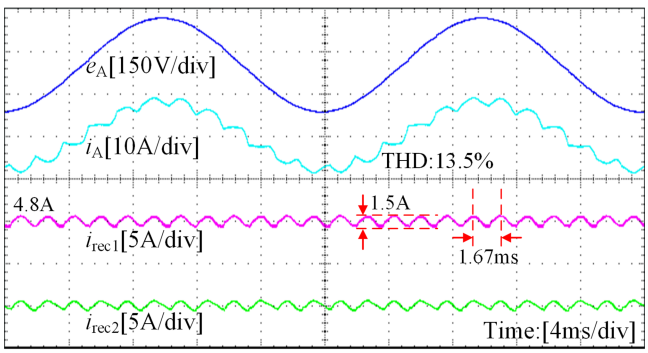

Fig. 40. Experimental waveforms of the 12-pulse rectifier without HRC in condition III.

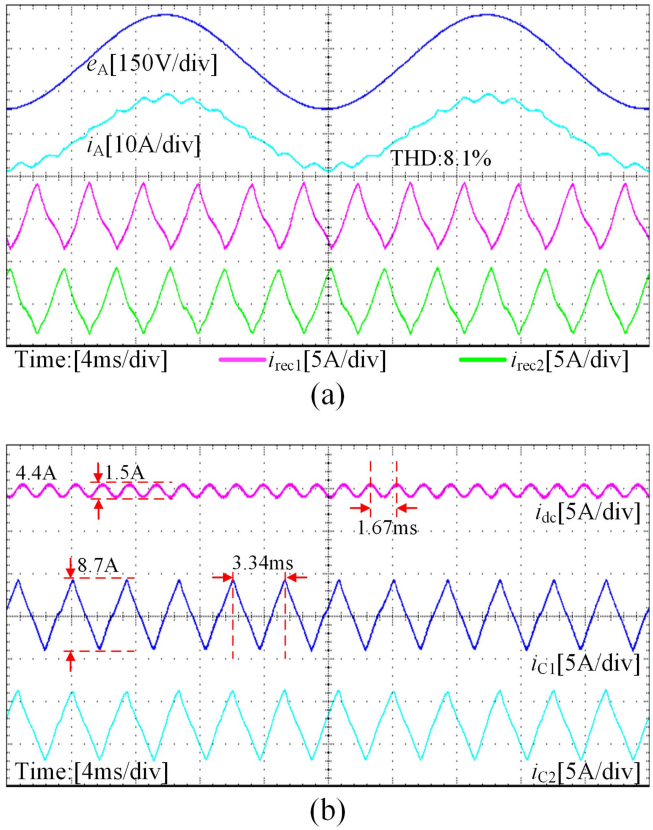

Fig. 41. Experimental waveforms of the existing 12-pulse rectifier with active HRC in condition III. (a) Input and output current waveforms of 12-pulse rectifier. (b) Load current $i_{\rm dc}$ and AHIC injection current i_{C1} and i_{C2}.

harmonic spectrum of the proposed rectifier at 100% and 20% rated power, and the harmonics meet IEEE-519 standard.

Condition IV: When two types of loads exist at the same time, i.e., a combination of operating conditions II and III, the experimental waveforms of the 12-pulse rectifier without HRC are shown in Fig. 44, and the THD of i_A is 14.1%. Fig. 45 illustrates the experimental waveforms of the existing 12-pulse rectifier with active HRC, and the THD of i_A up to 9.23%. Fig. 46 shows the experimental waveforms of the proposed 12-pulse rectifier with AHIC. The undesired harmonic suppression ability ensures a low THD of 2.59% for the i_A. Fig. 47 gives the i_A harmonic spectrum of the proposed rectifier at 100% and 20% rated power, and the THD meets IEEE-519 standard.

To verify the harmonic reduction effect of the proposed 12-pulse rectifier with AHIC under different load conditions, Fig. 48 illustrates input current THD comparison of 12-pulse rectifier without HRC, using active HRC and using proposed AHIC when load power changes from 20%P_L to 100%P_L under conditions I-IV. Under ideal load (conditions I), both AHIC and active HRC inject the same triangular currents and are able to significantly reduce the input current THD of the 12-pulse rectifier. In the presence of harmonics in the load current, the active HRC cannot compensate for the undesired harmonics in $i_{\rm rec1}$ and $i_{\rm rec2}$, resulting in rectifier input current THD that cannot meet the requirements. The proposed AHIC can offset the undesired harmonics of TPBRs outputs so that $i_{\rm rec1}$ and $i_{\rm rec2}$ are

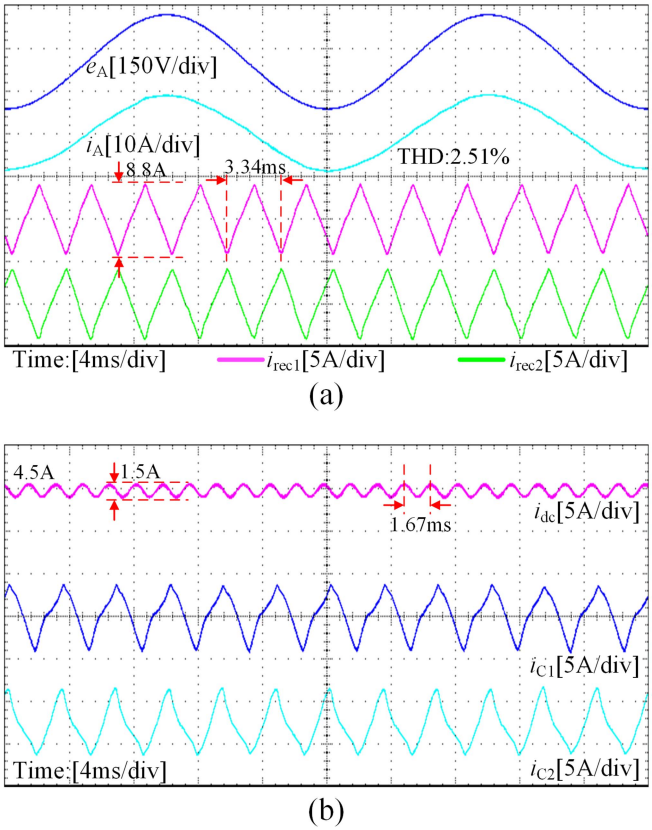

Fig. 42. Experimental waveforms of the proposed 12-pulse rectifier with AHIC in condition III. (a) Input and output current waveforms of 12-pulse rectifier. (b) Load current $i_{\rm dc}$ and AHIC injection current i_{C1} and i_{C2}.

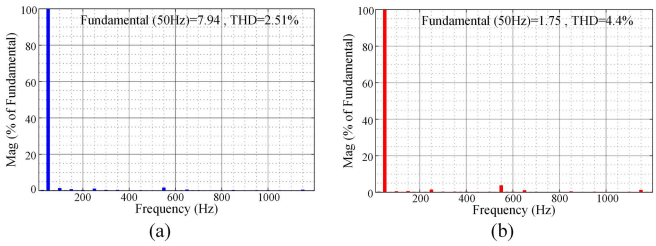

Fig. 43. Input current spectrum of the proposed rectifier in condition III. (a) 100%P_L. (b) 20%P_L.

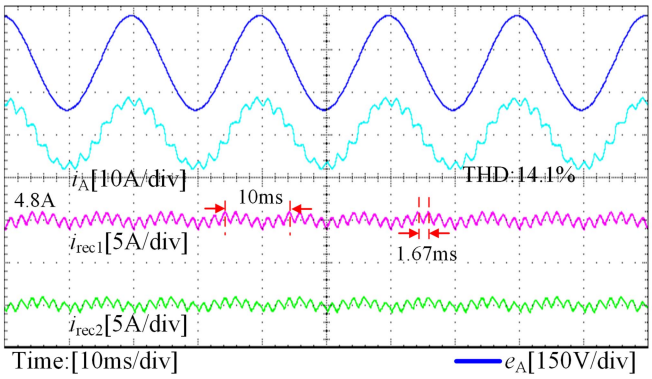

Fig. 44. Experimental waveforms of the 12-pulse rectifier without HRC in condition IV.

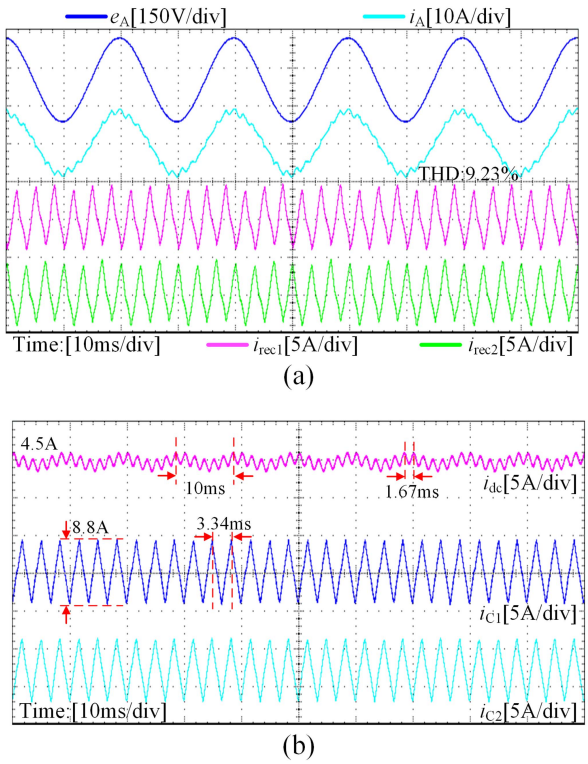

Fig. 45. Experimental waveforms of the existing 12-pulse rectifier with active HRC in condition IV. (a) Input and output current waveforms of 12-pulse rectifier. (b) Load current $i_{\rm dc}$ and AHIC injection current i_{C1} and i_{C2}.

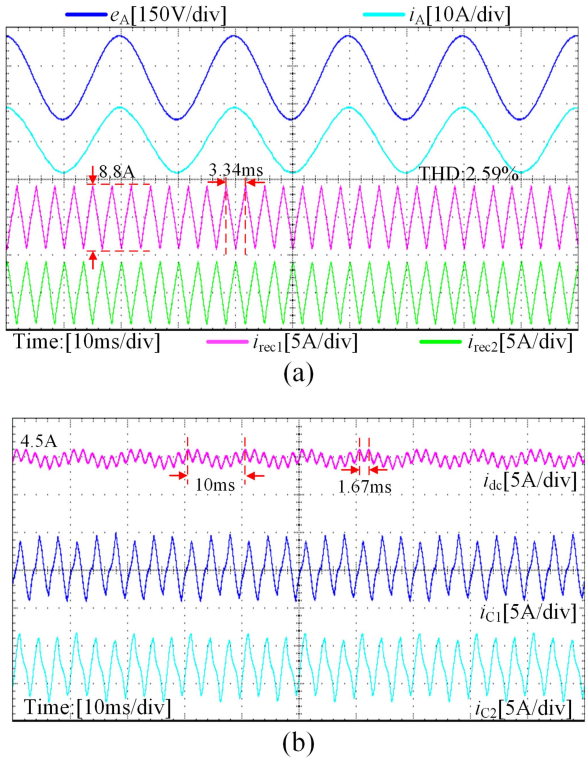

Fig. 46. Experimental waveforms of the proposed 12-pulse rectifier with AHIC in condition IV. (a) Input and output current waveforms of 12-pulse rectifier. (b) Load current $i_{\rm dc}$ and AHIC injection current i_{C1} and i_{C2}.

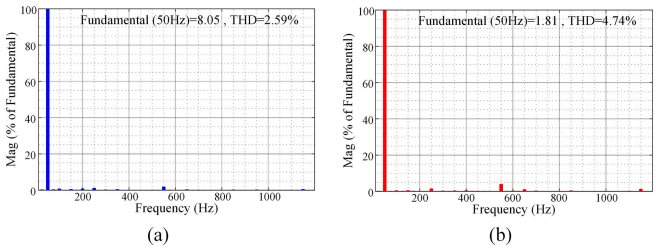

Fig. 47. Input current spectrum of the proposed rectifier in condition IV. (a) 100%P_L. (b) 20%P_L.

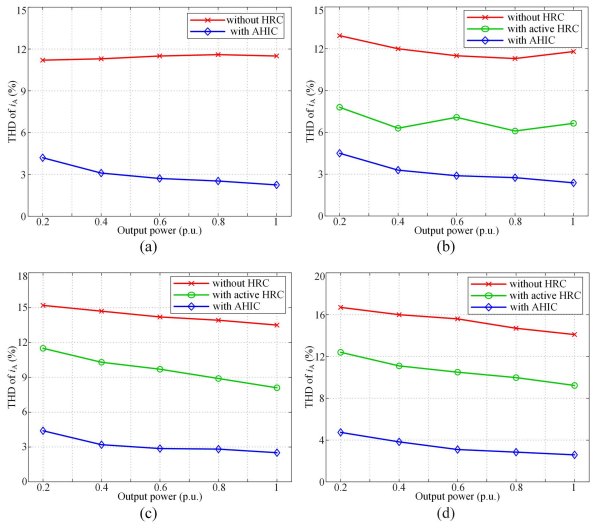

Fig. 48. Comparison of input current THD without HRC, with active HRC and with AHIC when load power changes from 0.2(p.u.) to 1(p.u.). (a) Under condition I. (b) Under condition II. (c) Under condition III. (d) Under condition IV.

ideal triangular currents, which ensures the input current quality under complex operating conditions with good load adaptability.

To further demonstrate the reliability of the proposed rectifier, dynamic performance tests were conducted. Fig. 49 shows the load transient dynamic experimental waveforms for the proposed 12-pulse rectifier with AHIC. It can be observed that when the load changes from 50% to 100%, the AHIC can stably output the triangular circulating current, effectively suppressing input current harmonics. Since the amplitude of the circulating current is obtained from $i_{\rm dc}$ after moving average filtering, the new circulating current command takes about two cycles to stabilize, which causes slight distortion in the input current during the transition process.

Fig. 50 shows the source voltage e_s transient dynamic experimental waveforms for the proposed 12-pulse rectifier with AHIC. When e_s drops by 10%, the AHIC can stably output a triangular circulating current, ensuring that the input current THD meets the standard requirements. Combining the above results, it is confirmed that the proposed AHIC can reliably suppress input current harmonics.

Fig. 51 shows the ratio of the loss caused by AHIC to total system power, it is clear that the introduced AHIC based on partial power compensation has little impact on the efficiency advantage of the 12-pulse rectifier. Due to the low power rating

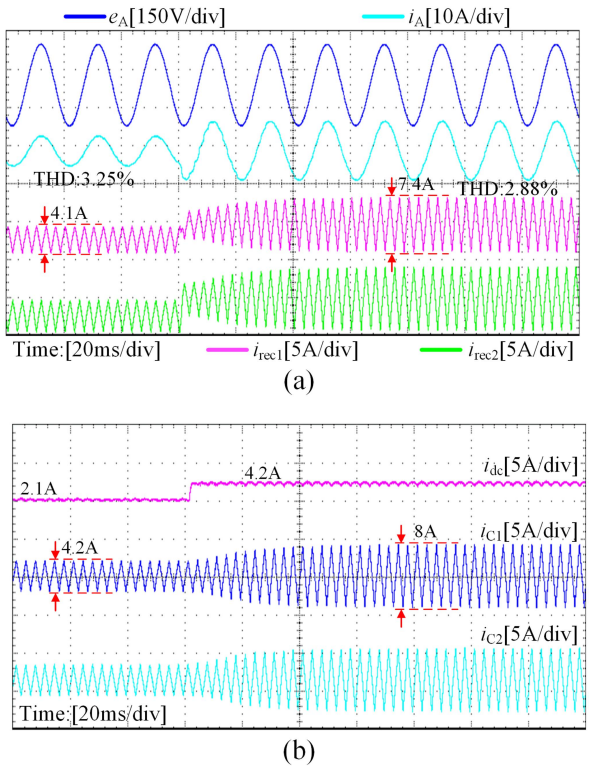

Fig. 49. Load transient dynamic experimental waveforms of proposed 12-pulse rectifier with AHIC. (a) Input and output current waveforms of 12-pulse rectifier. (b) Load current $i_{\rm dc}$ and AHIC injection current i_{C1} and i_{C2}.

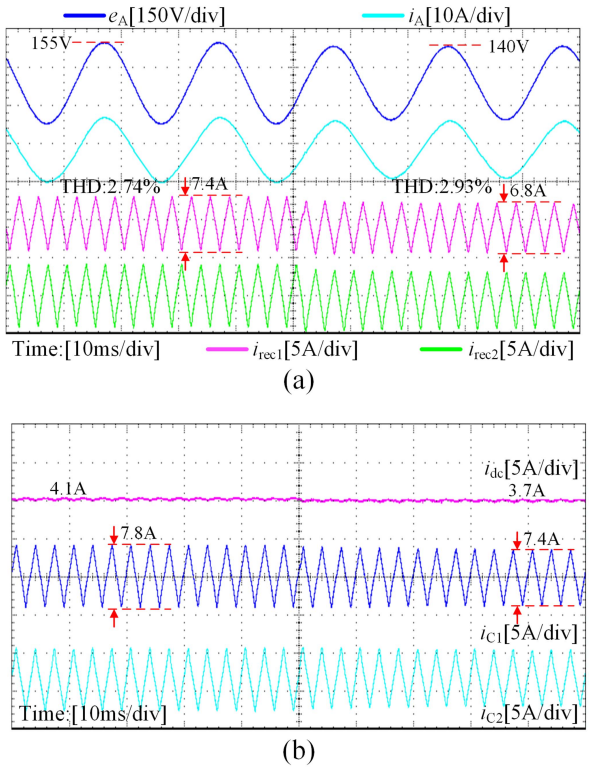

Fig. 50. Source voltage dynamic experimental waveforms of proposed 12-pulse rectifier with AHIC. (a) Input and output current waveforms of 12-pulse rectifier. (b) Load current $i_{\rm dc}$ and AHIC injection current i_{C1} and i_{C2}.

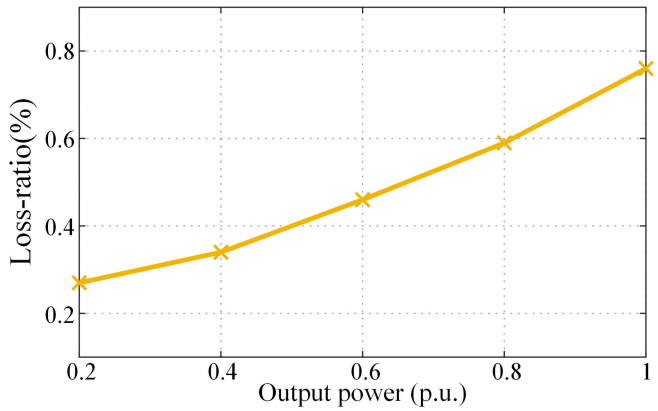

Fig. 51. Loss ratio of AHIC in prototype.

of the experimental prototype, the ideal loss ratio has not been achieved. As the power rating increases and the product development advances, the efficiency advantages of the proposed rectifier will become more pronounced.

VII. Conclusion

This article analyzes the load adaptability of the existing 12-pulse rectifier with active or passive HRCs. In order to overcome the poor input current harmonic suppression under nonideal load conditions by existing dc side harmonic reduction methods, a novel series-connected 12-pulse rectifier with AHIC is proposed. The harmonic suppression principle, controller, and system component design are given in detail. Then some conclusions can be obtained as follows:

1) The failure to compensate for the undesired harmonic currents at TPBRs output is the essence of the poor load adaptability of existing methods. Most existing HRCs have only one degree of freedom to control the injected triangular current, and the ideal ac current harmonic suppression can be guaranteed only when the $i_{\rm dc}$ is constant.
2) The two output currents of the proposed AHIC can be independently controlled, which are equivalent to two current sources. By superimposing the harmonic currents in $i_{\rm dc}$ on the triangular currents, the undesired harmonics of TPBRs are completely offset, and better harmonic suppression under practical load ripple current conditions is achieved, which improves the load adaptability of dc side harmonic reduction methods.
3) Using switch-multiplexing technology, the AHIC employs a two-stage dc–ac–ac three-port converter. Since the ports' voltage can be reduced as the outputs are in series with C_1 and C_2, the AHIC voltage rating is only $5\%U_{\rm dc}$ and the VA rating is only $2.5\%P_L$.
4) As the injection currents i_{C1} and i_{C2} are independently controlled, the IPR in traditional HRCs for equal current sharing is eliminated. In addition, the AHIC is directly connected to the system removing additional low-frequency auxiliary transformer.
5) The precise injection of specific harmonic currents is achieved in the $\alpha\beta$-frame. The method does not need to detect the input current harmonics of the 12-pulse rectifier, but only needs to sample the rectifier output voltage and load current to reduce the input current THD, and the control implementation is simple.

Finally, the experimental results verified that the proposed AHIC has greater load adaptability than the existing active HRC under conditions I-IV, and the system can operate stably during the dynamic process. The input current THD will be further reduced as the power level increases.

References

[1] D. Yuan, Z. Yin, S. Wang, and N. Duan, "Multi-level transient modeling of the aeronautic asymmetric 18-pulse phase-shifting auto-transformer rectifier in full-cycle design," *IEEE Trans. Transport. Electrific.*, vol. 8, no. 3, pp. 3759–3770, Sep. 2022.
[2] Q. Liu et al., "A compact-design oriented shipboard power supply system with transformer integrated filtering method," *IEEE Trans. Power Electron.*, vol. 37, no. 2, pp. 2089–2099, Feb. 2022.
[3] S. Sau and B. G. Fernandes, "Modular multilevel converter based variable speed drive with reduced capacitor ripple voltage," *IEEE Trans. Ind. Electron.*, vol. 66, no. 5, pp. 3412–3421, May 2019.
[4] B. Singh, S. Gairola, B. N. Singh, A. Chandra, and K. Al-Haddad, "Multipulse AC–DC converters for improving power quality: A review," *IEEE Trans. Power Electron.*, vol. 23, no. 1, pp. 260–281, Jan. 2008.
[5] X. Li, W. Xu, and T. Ding, "Damped high passive filter—A new filtering scheme for multi-pulse rectifier systems," *IEEE Trans. Power Del.*, vol. 32, no. 1, pp. 117–124, Feb. 2017.
[6] A. D. le Roux, H. D. T. Mouton, and H. Akagi, "DFT-based repetitive control of a series active filter integrated with a 12-pulse diode rectifier," *IEEE Trans. Power Electron.*, vol. 24, no. 6, pp. 1515–1521, Jun. 2009.
[7] H. Akagi and K. Isozaki, "A hybrid active filter for a three-phase 12-pulse diode rectifier used as the front end of a medium-voltage motor drive," *IEEE Trans. Power Electron.*, vol. 27, no. 1, pp. 69–77, Jan. 2012.
[8] J. Wang, A. Chen, X. Yao, L. Li, Y. Lv, and Q. Chen, "A simple 24-pulse rectifier employing an auxiliary pulse-doubling circuit," *IEEE Trans. Power Electron.*, vol. 37, no. 7, pp. 8392–8403, Jul. 2022.
[9] P. Kant and B. Singh, "A new three-phase to five-phase transformer with power quality improvement in hybrid-multilevel inverter based VCIMD," *IEEE Trans. Pow. Del.*, vol. 35, no. 2, pp. 871–880, Apr. 2020.
[10] A. de Oliveira Costa Neto, A. L. Soares, G. B. de Lima, D. B. Rodrigues, E. A. A. Coelho, and L. C. G. Freitas, "Optimized 12-pulse rectifier with generalized delta connection autotransformer and isolated sepic converters for sinusoidal input line current imposition," *IEEE Trans. Power Electron.*, vol. 34, no. 4, pp. 3204–3213, Apr. 2019.
[11] S. P. P. R.Kalpana, B. Singh, and G. Bhuvaneswari, "A 20-pulse asymmetric multi-phase staggering autoconfigured transformer for power quality improvement," *IEEE Trans. Power Electron.*, vol. 33, no. 2, pp. 917–925, Feb. 2018.
[12] T. Wang, F. Fang, X. Jiang, K. Wang, and L. Yang, "Performance and design analysis on round-shaped transformers applied in rectifier systems," *IEEE Trans. Ind. Electron.*, vol. 64, no. 2, pp. 948–955, Feb. 2017.
[13] R. Abdollahi, G. B. Gharehpetian, A. Anvari-Moghaddam, and F. Blaabjerg, "A 40-pulse autotransformer rectifier based on new pulse multiplication circuit for aviation application," *IEEE Trans. Ind. Electron.*, vol. 70, no. 11, pp. 10822–10832, Nov. 2023.
[14] Q. Du, L. Gao, Q. Li, W. Liu, X. Yin, and F. Meng, "Harmonic reduction methods at DC link of series-connected multi-pulse rectifiers: A review," *IEEE Trans. Power Electron.*, vol. 37, no. 3, pp. 3143–3160, Mar. 2022.
[15] S. Choi, J. Oh, K. Kim, and J. Cho, "A new 24-pulse diode rectifier for high voltage and high power applications," in *Proc. 30th Annu. IEEE Power Electron. Specialists Conf. Rec.*, 1999, pp. 169–174.
[16] Y. Nishida and M. Nakaoka, "A new harmonic reducing three-phase diode rectifier for high voltage and high power applications," in *Proc. IEEE Ind. Appl. Conf. 32nd IAS Annu. Meeting*, 1997, pp. 1624–1632.
[17] J. Wang, Y. Lv, L. Li, X. Yao, Q. Guan, and Q. Chen, "A 24-pulse rectifier with a passive auxiliary current injection circuit at DC side," *IEEE Trans. Power Electron.*, vol. 37, no. 9, pp. 11109–11123, Sep. 2022.
[18] J. Wang et al., "A series-connected 24-pulse AC–DC converter with double-diode harmonic suppression circuit," *IEEE Trans. Power Electron.*, vol. 38, no. 4, pp. 5240–5253, Apr. 2023.

[19] J. Wang, C. Zhao, T. Yu, T. Liu, X. Yao, and Q. Chen, "New 24-pulse rectifier with passive current injection circuit based on dual auxiliary transformers," *IEEE J. Emerg. Sel. Topics Power Electron.*, vol. 11, no. 5, pp. 5321–5336, Oct. 2023.
[20] J. Wang, A. Chen, L. Li, C. Zhao, X. Yao, and Q. Chen, "A simple 36-pulse rectifier with passive pulse-tripling circuit at the DC side," *IEEE Trans. Ind. Electron.*, vol. 70, no. 1, pp. 17–28, Jan. 2023.
[21] S. Choi, J. Oh, and J. Cho, "Multi-pulse converters for high voltage and high power applications," in *Proc. IEEE Power Electron. Motion Control Conf.*, 2000, vol. 3, pp. 1019–1024.
[22] M. Villablanca, M. Arias, and C. Acevedo, "High-pulse series converters for HVDC systems," *IEEE Trans. Power Del.*, vol. 16, no. 4, pp. 766–774, Oct. 2001.
[23] F. Meng, Q. Du, L. Wang, L. Gao, and Z. Man, "A series-connected 24-pulse rectifier using passive voltage harmonic injection method at DC-link," *IEEE Trans. Power Electron.*, vol. 34, no. 9, pp. 8503–8512, Sep. 2019.
[24] Q. Li, F. Meng, L. Gao, H. Zhang, and Q. Du, "A 30-pulse rectifier using passive voltage harmonic injection method at DC link," *IEEE Trans. Ind. Electron.*, vol. 67, no. 11, pp. 9273–9291, Nov. 2020.
[25] F. Meng, T. Li, L. Wang, and L. Gao, "Series-connected 36-pulse rectifier using a hybrid harmonic injection method," *IET Power Electron*, vol. 13, no. 17, pp. 4112–4116, Dec. 2020.
[26] Q. Du, W. Liu, Q. Li, L. Gao, and F. Meng, "A series-connected 40-pulse rectifier with DC link passive harmonic reduction circuit," *IEEE Trans. Power Electron.*, vol. 37, no. 3, pp. 3007–3023, Mar. 2022.
[27] Q. Li, Q. Du, X. Yin, L. Gao, and F. Meng, "General injection transformer turn ratio design method and hybrid harmonic reduction methods for series-connected multipulse rectifiers," *IEEE Trans. Power Electron.*, vol. 37, no. 12, pp. 15457–15468, Dec. 2022.
[28] M. E. Villablanca, J. I. Nadal, F. A. Cruzat, and W. C. Rojas, "Harmonic improvement in 12-pulse series-connected line-commutated rectifiers," *IET Power Electron.*, vol. 2, no. 4, pp. 466–473, Jul. 2009.
[29] M. M. Swamy, "An electronically isolated 12-pulse autotransformer rectification scheme to improve input power factor and lower harmonic distortion in variable-frequency drives," *IEEE Trans. Ind. Appl.*, vol. 51, no. 5, pp. 3986–3994, Sep./Oct. 2015.
[30] S. Bai and S. M. Lukic, "New method to achieve AC harmonic elimination and energy storage integration for 12-pulse diode rectifiers," *IEEE Trans. Ind. Electron.*, vol. 60, no. 7, pp. 2547–2554, Jul. 2013.
[31] S. Fukuda, M. Ohta, and Y. Iwaji, "An auxiliary-supply-assisted harmonic reduction scheme for 12-pulse diode rectifiers," *IEEE Trans. Power Electron.*, vol. 23, no. 3, pp. 1270–1277, May 2008.
[32] F. Meng, W. Yang, S. Yang, and L. Gao, "Active harmonic reduction for 12-pulse diode bridge rectifier at DC side with two-stage auxiliary circuit," *IEEE Trans. Ind. Informat.*, vol. 11, no. 1, pp. 64–73, Feb. 2015.
[33] V. Sheelvant, R. Kalpana, B. Singh, and P. P. Saravana, "Improvement in harmonic reduction of a zigzag autoconnected transformer based 12-pulse diode bridge rectifier by current injection at DC side," *IEEE Trans. Ind. Appl.*, vol. 53, no. 6, pp. 5634–5644, Nov./Dec. 2017.
[34] F. Meng, W. Yang, Y. Zhu, L. Gao, and S. Yang, "Load adaptability of active harmonic reduction for 12-pulse diode bridge rectifier with active interphase reactor," *IEEE Trans. Power Electron.*, vol. 30, no. 12, pp. 7170–7180, Dec. 2015.
[35] F. Liu, X. Ruan, X. Huang, and Y. Qiu, "Second harmonic current reduction for two-stage inverter with DCX-LLC resonant converter in front-end DC/DC converter: Modeling and control," *IEEE Trans. Power Electron.*, vol. 36, no. 4, pp. 4597–4609, Apr. 2021.
[36] R. Sun et al., "A DC bus oscillation suppression strategy based on series voltage compensator for diode rectifier," *IEEE Trans. Power Electron.*, vol. 39, no. 5, pp. 5207–5224, May 2024.
[37] J. Liu and Y. Zhang, "Current pulsation suppression method based on power current closed-loop control for a PMSM under fluctuating DC-link voltage," *IEEE Trans. Power Electron.*, vol. 37, no. 1, pp. 761–770, Jan. 2022.
[38] Y. Wu, W. Wang, F. Tang, and X. Wu, "Adaptive virtual admittance control of bidirectional DC/DC converters for dc bus voltage ripple suppression in dc microgrids," *Int. J. Electr. Power Energy Syst.*, vol. 159, Aug. 2024, Art. no. 110045.
[39] Y. Wu et al., "Improved model predictive current control for multi-mode four-switch buck-boost converter considering parameter mismatch," *IET Power Electron.*, vol. 16, no. 6, pp. 1043–1062, May 2023.
[40] T. Wang and S. Lu, "Analysis of the DC-link current for the single-phase H-bridge inverter under harmonic output currents," *IEEE J. Emerg. Sel. Topics Power Electron.*, vol. 7, no. 4, pp. 2170–2183, Dec. 2019.

Ruidong Sun (Student Member, IEEE) was born in Yuncheng, China. He received the B.S. degree in electrical engineering from North University of China, Taiyuan, China, in 2018, and the M.S. degree in electrical engineering from Beijing Jiaotong University, Beijing, China, in 2020. He is currently working toward the Ph.D. degree in electrical engineering with the School of Electrical Engineering, Beijing Jiaotong University, Beijing, China.

His current research interests include hybrid rectifier, dc–dc converters, and renewable power generation.

Guohong Zeng received the B.S. degree in power drive control, the M.S. degree in power electronics and power drives, and the Ph.D. degree in automation of electric power system from Beijing Jiaotong University, Beijing, China, in 1988, 1991, and 2003, respectively.

He is currently an Associate Professor with the School of Electrical Engineering, Beijing Jiaotong University. His general research interests include power quality theory and improvement technology, high-power motor control technology, renewable energy, and energy storage technology.

Buyu Yang was born in Zibo, China. He received the B.S. degree in electrical engineering and automation from Qingdao University of Technology, Qingdao, China, in 2024. He is currently working toward the M.S. degree in electrical engineering with the School of Electrical Engineering, Beijing Jiaotong University, Beijing, China.

His current research interests include hybrid rectifier, and dc–ac converters.

Luoqi Wu received the B.S. degree in electrical engineering from Xi'an University of Technology, Shaanxi, China, in 2022. He is currently working toward the M.S. degree in electrical engineering with the School of Electrical Engineering, Beijing Jiaotong University, Beijing, China.

His current research interest focuses on high-power rectifier.

Wenzheng Xu received the B.Eng. degree in electrical engineering from Beijing Jiaotong University, Beijing, China, in 2012, the M.Sc. degree (with Distinction) in energy engineering from The University of Hong Kong, Hong Kong, in 2013, and the Ph.D. degree in electrical engineering from The Hong Kong Polytechnic University (PolyU), Hong Kong, in 2020.

From September 2013 to June 2015 and March to June 2020, he was a Research Assistant and a Postdoctoral Fellow respectively with the Department of Electrical Engineering, PolyU, working on high-power converters and fast-charging devices for electric vehicles. He is currently a Lecturer with School of Electrical Engineering, Beijing Jiaotong University. His research interests include power electronics, wireless power transfer, transportation electrification, and energy interconnection.

Long Jing was born in Urumqi, China. He received the B.S., M.S., and Ph.D. degrees from Beijing Jiaotong University, Beijing, China, in 1999, 2002, and 2008, respectively, all in electrical engineering.

He is currently an Associate Professor with the School of Electrical Engineering, Beijing Jiaotong University. He has been engaged in the teaching and research of power electronics technology and new energy power generation. His current research interests include different ac/dc, dc/dc converters for energy storage, battery system control strategies, modular multilevel converters, etc.

Xuezhi Wu (Member, IEEE) received the B.S. and M.S. degrees in electrical engineering from Beijing Jiaotong University, Beijing, China, in 1996 and 1999, respectively, and the Ph.D. degree in electrical engineering from Tsinghua University, Beijing, China, in 2003.

He is currently a Professor with the School of Electrical Engineering, Beijing Jiaotong University. His current research interests include microgrids, wind power generation systems, power converters for renewable generation systems, power quality, and motor control.

Jianhua Lei received the B.S. degree in automation from Beihua University, Jilin, China, in 2008, and the M.S. degree in materials engineering from Sun Yat-sen University, Guangzhou, China, in 2015. He is currently working toward the Ph.D. degree in materials and chemical engineering with Tsinghua University, Shenzhen, China.

He joined the Shenzhen Poweroak Newener Company Ltd., Shenzhen, China, as Chief Technology Officer, in June 2018. His current research interests include power electronic switching power supply control technologies, energy storage inverter technologies, and renewable energy-based water electrolysis for hydrogen production.

Yongbo Zhang received the M.Eng. degree in electrical engineering from Beijing Jiaotong University, Beijing, China, in 2015.

He has been the R&D Director with Shenzhen Poweroak Newener Company Ltd., Shenzhen, China, since 2021. His current research interests include renewable energy generation systems, power electronics for energy storage inverters, and advanced digital power supply design.